ARTICLE

Ultra-large library docking for discovering new chemotypes

Jiankun Lyu[1,2,10], Sheng Wang[3,4,10], Trent E. Balius[1,10], Isha Singh[1,10], Anat Levit[1], Yurii S. Moroz[5,6], Matthew J. O'Meara[1], Tao Che[4], Enkhjargal Algaa[1], Kateryna Tolmachova[7], Andrey A. Tolmachev[7], Brian K. Shoichet[1]*, Bryan L. Roth[4,8,9]* & John J. Irwin[1]*

Despite intense interest in expanding chemical space, libraries containing hundreds-of-millions to billions of diverse molecules have remained inaccessible. Here we investigate structure-based docking of 170 million make-on-demand compounds from 130 well-characterized reactions. The resulting library is diverse, representing over 10.7 million scaffolds that are otherwise unavailable. For each compound in the library, docking against AmpC β-lactamase (AmpC) and the D_4 dopamine receptor were simulated. From the top-ranking molecules, 44 and 549 compounds were synthesized and tested for interactions with AmpC and the D_4 dopamine receptor, respectively. We found a phenolate inhibitor of AmpC, which revealed a group of inhibitors without known precedent. This molecule was optimized to 77 nM, which places it among the most potent non-covalent AmpC inhibitors known. Crystal structures of this and other AmpC inhibitors confirmed the docking predictions. Against the D_4 dopamine receptor, hit rates fell almost monotonically with docking score, and a hit-rate versus score curve predicted that the library contained 453,000 ligands for the D_4 dopamine receptor. Of 81 new chemotypes discovered, 30 showed submicromolar activity, including a 180-pM subtype-selective agonist of the D_4 dopamine receptor.

In a highly cited footnote, Bohacek and colleagues suggested that there are over 10^{63} drug-like molecules[1]. This is too many to even enumerate, and other estimates of drug-like chemical space have been proposed[2–4]. What is clear is that the number of possible drug-like molecules is many orders of magnitude higher than the number that exists in early discovery libraries, and that this number grows exponentially with molecular size[3]. Because most optimized chemical probes and drug candidates resemble the initial discovery hit[5], there is much interest in expanding the number of molecules and chemotypes that can be explored in early screening.

Expanding chemical space

An early effort to enlarge chemical libraries focused on the enumeration of side chains from central scaffolds. Although such combinatorial libraries can be very large, efforts to produce and test them often suffered from problems with compound synthesis, assay artefacts[6] and a lack of diversity. More recently, a related strategy using DNA-encoded libraries[7] has overcome many of these deficits[8]. Still, most DNA-encoded libraries are limited to several reaction types or core scaffolds[9], reducing diversity.

In principle, structure-based docking can screen virtual libraries of great size and diversity, selecting only the best-fitting molecules for synthesis and testing. These advantages are balanced by serious deficits: docking cannot calculate the affinity of a compound accurately[10] and the technique has many false-positive hits. Accordingly, docking of readily available molecules is crucial. For virtual molecules, such accessibility has been problematic. Worse still, a large library screen could exacerbate latent docking problems, giving rise to new false-positive hits. Thus, although docking screens of several million

molecules have found potent ligands for multiple targets[11–22], docking much larger virtual libraries has remained largely speculative.

To overcome the problem of compound availability in a make-on-demand library, we focused on molecules from 130 well-characterized reactions using 70,000 building blocks from Enamine (Fig. 1). The resulting reaction products are often functionally congested—displaying multiple groups from a compact scaffold—with substantial three-dimensionality; less than 3% are commercially available from another source. The addition of new reactions and building blocks has steadily grown the library (Fig. 1a). At the time of publication, there are over 350 million make-on-demand molecules in ZINC (http://zinc15.docking.org) in the lead-like range[23]. More than 1.6 billion readily synthesizable molecules have been enumerated, and the dockable library should soon grow beyond 1 billion molecules (Fig. 1b). Meanwhile, diversity is retained: a new scaffold is added for approximately every 20 new compounds (Fig. 1c). As a consequence of its great size and diversity, a library of this size is almost entirely virtual.

Even if the make-on-demand molecules are readily accessible, a combination of inaccurate scores and a vast chemical space could overwhelm the true active compounds with docking decoys. Accordingly, we simulated how hit rates would vary as the library grew from tens-of-thousands to hundreds-of-millions of molecules. First, we docked tens-to-hundreds of known ligands mixed with thousands of property-matched decoys[24] (Extended Data Fig. 1a, b). From the resulting rank distributions, we simulated the effect of varying the ligand-to-decoy ratio in a growing library. Performance was judged by the number of ligands in the top 1,000 ranked molecules for any library size, a stringent criterion. When ligands were enriched in the smaller libraries, performance typically improved with library size (Extended

[1]Department of Pharmaceutical Chemistry, University of California, San Francisco, San Francisco, CA, USA. [2]State Key Laboratory of Bioreactor Engineering, Shanghai Key Laboratory of New Drug Design, School of Pharmacy, East China University of Science & Technology, Shanghai, China. [3]State Key Laboratory of Molecular Biology, CAS Center for Excellence in Molecular Cell Science, Shanghai Institute of Biochemistry and Cell Biology, Chinese Academy of Sciences, University of Chinese Academy of Sciences, Shanghai, China. [4]Department of Pharmacology, University of North Carolina at Chapel Hill School of Medicine, Chapel Hill, NC, USA. [5]National Taras Shevchenko University of Kiev, Kiev, Ukraine. [6]Chemspace, Riga, Latvia. [7]Enamine, Kiev, Ukraine. [8]Division of Chemical Biology and Medicinal Chemistry, Eshelman School of Pharmacy, University of North Carolina at Chapel Hill, Chapel Hill, NC, USA. [9]National Institute of Mental Health Psychoactive Drug Screening Program (NIMH PDSP), School of Medicine, University of North Carolina at Chapel Hill School of Medicine, Chapel Hill, NC, USA. [10]These authors contributed equally: Jiankun Lyu, Sheng Wang, Trent E. Balius, Isha Singh. *e-mail: bshoichet@gmail.com; bryan_roth@med.unc.edu; jir322@gmail.com
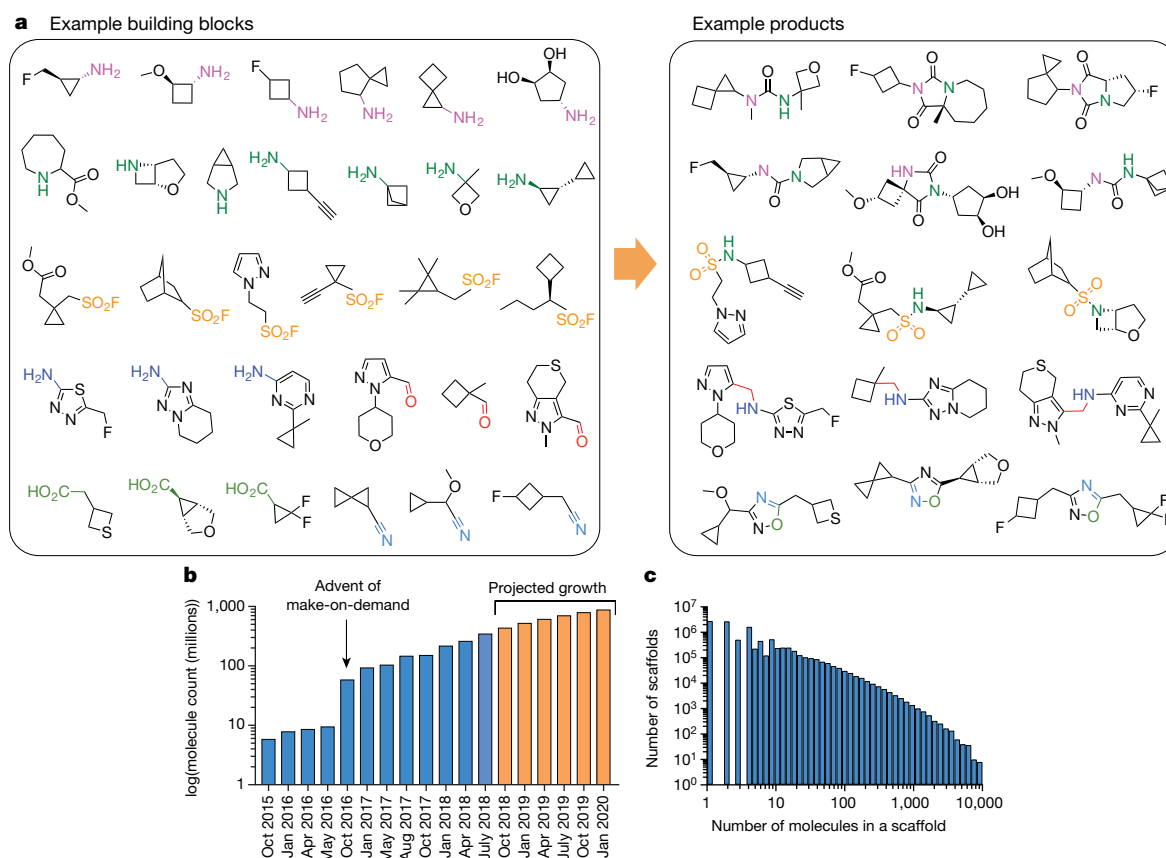
Fig. 1 | Make-on-demand compounds are diverse and have increased exponentially. a, Characteristic reagents, reactions and products in the make-on-demand library. **b**, The expansion of the make-on-demand library; orange bars represent projected growth. **c**, The distribution of compounds among the 10.7 million scaffolds in the library.

Data Fig. 1c). Conversely, when docking performed poorly in small benchmarks, performance often deteriorated with library size.

Second, we investigated ligand enrichment against the full make-on-demand library. We counted known binding compounds as well as their close analogues in the library as ligands; the rest of the library was considered to be decoys (Methods). For targets with well-formed binding sites, known ligands and ligand analogues were found among the top docking hits, even in libraries of more than 170 million molecules (Extended Data Fig. 1d and Supplementary Table 1).

Docking 99 million molecules against AmpC

Encouraged by these simulations, we turned to prospective prediction of new compounds. We targeted two unrelated proteins: the enzyme AmpC and the D_4 dopamine (D_4) receptor. Against AmpC, we docked the make-on-demand lead-like library, which was—at the time—composed of 99 million molecules. Each compound was fit in the enzyme active site with an average of 4,054 orientations, and for each orientation 280 conformations were sampled. Each configuration was scored for energetic fit, using the physics-based DOCK3.7 scoring function. The top-ranked 1 million molecules were clustered by scaffold[25] and by topological similarity, reducing redundancy. Molecules were excluded that resembled known AmpC inhibitors from ChEMBL[26] (ECFP4 Tanimoto coefficient (Tc) > 0.45) or that resembled any molecule in the 3.5 million in-stock library (ECFP4 Tc > 0.5). Therefore, we sought molecules that were newly generated and matched to the enzyme.

Fifty-one top-ranking molecules—each a different scaffold—were selected for testing, of which 44 (86%) were successfully synthesized (Supplementary Table 9 and Supplementary Data 11, 12). Five compounds measurably inhibited AmpC, with inhibitory constant (K_i) values ranging from 1.3 to 400 μM (Extended Data Figs. 2, 3), constituting an 11% hit rate. All five compounds were selective competitive inhibitors that did not aggregate, nor did they inhibit counter-screening enzymes such as trypsin and chymotrypsin (Supplementary Tables 2, 3). Notably, the compound ZINC339204163 at 1.3 μM engages the crucial oxyanion hole of AmpC with a phenolate. Not only is 339204163 the most potent reversible AmpC inhibitor found in any screen of which we are aware, but also its phenolate is a warhead that is rarely—if ever—known to interact with β-lactamases, and is one with few precedents among inhibitors of other amidases and proteases[27]. To optimize the five initial hits, we chose 90 well-scoring analogues from within the make-on-demand library (Methods). Over half were active on testing, improving the affinity of each of the 5 hits by 3- to 29-fold (Extended Data Fig. 2 and Supplementary Table 2). This included the compound ZINC549719643 (77 nM), an analogue of the phenolate 339204163, which is among the most potent non-covalent AmpC inhibitors of which we are aware. The ability to optimize affinity by finding analogues within the library attests to its depth of coverage for many chemotypes.

Crystal structures of three of the new ligand families, and of 549719643 at 77 nM, were determined to a resolution that ranged from 1.50 to 1.91 Å. Unambiguous electron density maps confirmed their fidelity to the docking predictions, with root mean square deviation (r.m.s.d.) values that varied from 0.98 to 1.52 Å (Fig. 2, Extended Data Table 1 and Extended Data Fig. 4). The r.m.s.d. increases to 1.98 Å for ZINC275579920; however, this largely reflects a rotation of the terminal ring, which makes no polar interactions with the enzyme in either conformation. For the central core of 275579920, the r.m.s.d. is 1.20 Å and all five hydrogen bonds predicted by docking are found in the crystal structure (Fig. 2b). Such polar interactions corresponded well between docked and crystallographic poses in all four structures, including that of the phenolate of 549719643, which forms the three docking-predicted hydrogen bonds with the oxyanion hole of AmpC (Fig. 2e).
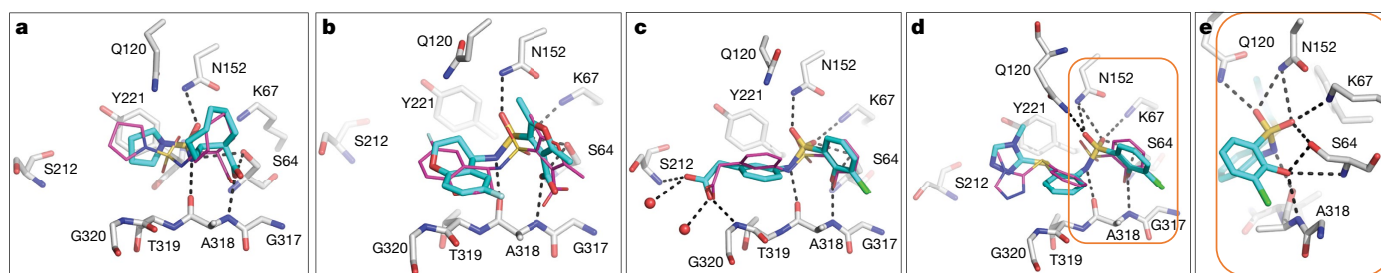
Fig. 2 | Structural fidelity between docked-predicted and crystallographically determined poses of the new β-lactamase inhibitors. Crystal structures of the inhibitors (carbons in cyan) overlaid with their docking predictions (magenta). AmpC carbon atoms are shown in grey, oxygens in red, nitrogens in blue, sulfurs in yellow, chlorides in green and fluorides in light blue. Hydrogen bonds are shown as black dashed lines. **a–d**, AmpC in complex with ZINC547933290 (**a**; Protein Data Bank (PDB) 6DPZ, r.m.s.d. = 1.3 Å) and 275579920 (**b**; PDB 6DPY, r.m.s.d. = 1.2 Å for the warhead), the 1.3 μM inhibitor 339204163 (PDB 6DPX; r.m.s.d. = 0.98 Å) and its 77 nM analogue 549719643 (**d**; PDB 6DPT, r.m.s.d. = 1.52 Å). **e**, Close-up of the 549719643 phenolate in the oxyanion hole. Extended Data Fig. 4 shows the electron densities.

Docking 138 million molecules against the D₄ receptor

The prospective screen against the D$_4$ receptor had two goals. The first was to see whether we could discover new receptor chemotypes, as with most docking investigations. A second goal was to investigate something that remains largely unexplored in molecular docking: how success varies with docking rank. Accordingly, we tested 549 make-on-demand molecules drawn from not only high-ranking molecules, but also from mid- and low-ranked ones (Fig. 3a).

Seeking new chemotypes[28,29], 138 million library molecules were docked against the structure of the receptor[14]. About 70 trillion complexes were sampled in the orthosteric site, requiring 43,563 core hours or about 1.2 calendar days on 1,500 cores. Again, the ranked library was clustered by topology and by scaffold[25], reducing redundancy. To increase novelty, molecules found in the 3.5 million in-stock library, or that resembled the approximately 28,000 dopaminergic, serotonergic or adrenergic ligands in ChEMBL (https://www.ebi.ac.uk/chembl/) (Tc ≥ 0.35 by ECFP4 fingerprints), were excluded. Of the 589 molecules selected, 549 (93%) were successfully synthesized (Supplementary Table 10 and Supplementary Data 11, 13). From the top 1,000 ranking clusters, 124 molecules were selected by visual inspection for favourable and diverse interactions with the D$_4$ site and for lack of internal strain[30]; another 444 were selected automatically, by docking score alone, across the rank-ordered list (19 were in both lists). At 10 μM, 122 of the 549 molecules displaced more than 50% ³H-*N*-methylspiperone-specific D$_4$ receptor binding (Fig. 3a). Dose–response curves for 81 compounds revealed K_i values that ranged from 18.4 nM to 8.3 μM (Fig. 3b, Extended Data Table 2 and Supplementary Table 4).

Many of the highly ranked molecules were functionally congested, and often docked to interact with residues that are rarely simultaneously engaged (Fig. 3c and Extended Data Fig. 5). Most filled the pocket defined by residues in helices 5 and 6, such as S196[5.42], F410[6.51] and F411[6.52], and ion-paired with D115[3.32], both common interactions among dopaminergic ligands (Fig. 3c, superscripts use Ballesteros–Weinstein and GPCRdb nomenclature[31,32]). Less common among previously known ligands, but frequently observed here, was engagement of the D$_4$ receptor selectivity pocket, defined by F91[2.61] and L111[3.28], which distinguishes this subtype from the D$_2$ and D$_3$ dopamine receptors (Fig. 3c). This may explain the 30- to 500-fold subtype selectivity of many of the hits (Extended Data Table 2). Finally, some compounds docked to further hydrogen-bond with backbone atoms in extracellular loop 2 (Fig. 3c), which is thought to influence signalling bias[33].

In functional assays, several of the high-ranking molecules were potent. For instance, ZINC621433143 appeared to be a full agonist at 2.3 nM (see below), ZINC465129598 and ZINC270269326 were full agonists at 24 nM and 17 nM, respectively, whereas ZINC464771011 was a partial agonist at 10 nM (Fig. 3d and Extended Data Table 2). Two antagonists were also found: ZINC413570733 (half-maximum inhibitory concentration (IC$_{50}$) = 5.9 μM) and ZINC130532671 (IC$_{50}$ = 10.8 μM) (Extended Data Table 2 and Extended Data Fig. 5). All six compounds lacked detectable activity against the D$_2$ or D$_3$

dopamine receptor subtypes (Extended Data Table 2). Meanwhile, ZINC615622500 had no detectable G$_i$ activity, but was a β-arrestin-biased agonist at 3 μM (Extended Data Table 2 and Extended Data Fig. 5).

Notably, the potent agonist 21433143 was tested as a diastereomeric mixture. Several of its diastereomers, each independently docked, also scored well—an example is ZINC621433144, which differs from 21433143 by adopting the (3*R*, 4*S*) rather than the (3*S*, 4*S*) stereoisomer around the tetrahydropyrrole; the two stereoisomers superpose well onto their docked poses on the D$_4$ receptor (Fig. 3c). Accordingly, the four diastereomers were independently synthesized and tested. Compound 621433144 is a full agonist at 180 pM, with 2,500-fold subtype selectivity, making it one of the most potent, selective full agonists characterized for the D$_4$ receptor. Compound 621433144 was also functionally selective, with a 17-fold bias towards G$_i$ signalling versus β-arrestin recruitment, compared to the characteristic agonist quinpirole (Fig. 3e). Two of the other diastereomers, ZINC361131264 and ZINC361131265, had G$_i$ biases of 26- and 11-fold, respectively, and the third (21433143) had a β-arrestin bias of 7-fold (Extended Data Table 2); here stereoisomerization at a single centre flips the bias of a potent agonist.

The make-on-demand library will soon exceed one billion lead-like molecules (Fig. 1b), and it is tempting to dock only cluster representatives, rather than every single molecule. Indeed, doing so reduced docking time by 22-fold. Unfortunately, the best cluster representative for a protein is unknowable without docking all cluster members. We found that only docking a single cluster representative, chosen by multiple criteria (Methods), substantially reduced the docking scores, especially for the highest-ranked molecules (Fig. 3f and Extended Data Fig. 6a). This had a devastating effect on experimentally active scaffold families. For instance, the 47 confirmed active compounds among the top 3,000 ranked molecules were replaced with different cluster representatives, and these fell in rank by an average of 1,121,443; only 2 of the original active scaffolds remained (Supplementary Table 7). Similar effects were observed for β-lactamase (Extended Data Fig. 6b and Supplementary Table 8). Screening the entire library was essential for the discovery of the compounds that we report here.

Docking hit rates vary regularly with score

A longstanding question in docking is how well rank predicts binding likelihood. In most docking screens, only tens of molecules are tested, and then only from among the top ranks. With the great expansion of the library, it seemed interesting to sample also from lower ranks, with enough molecules to be statistically meaningful. Accordingly, we modelled potential 'hit-rate' curves as a function of docking score. Using distributions of prior probabilities from Bayesian statistics, we developed ranges of docking scores over which we should test molecules to experimentally define the curve (Fig. 4). From these simulations, the 549 make-on-demand molecules were spread among 12 scoring bins covering the highest-ranking (−75 to −63 kcal mol⁻¹), mid-ranking (−61 to −46 kcal mol⁻¹) and low-ranking scores, for which
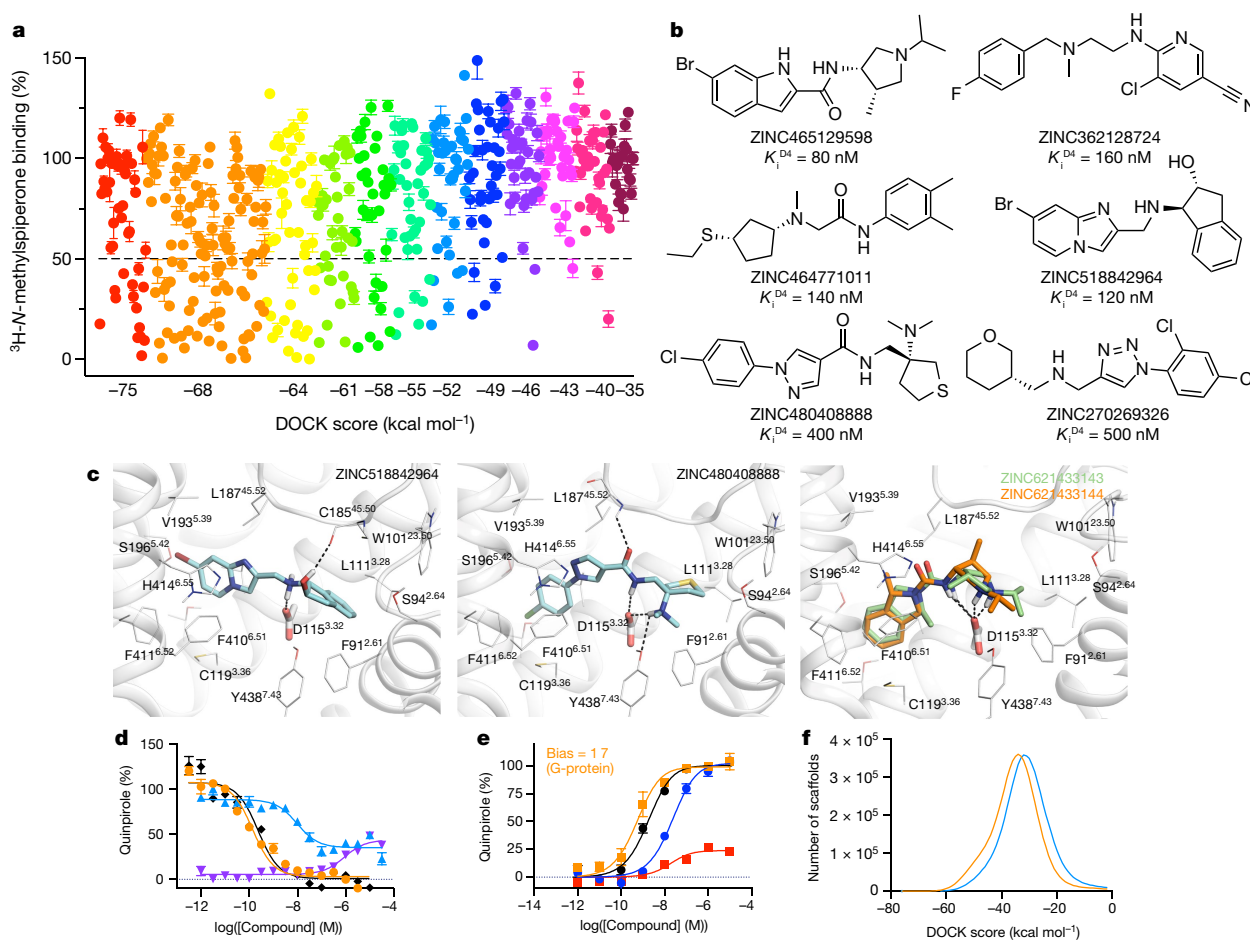
Fig. 3 | Testing 549 molecules at different docking ranks against the D₄ receptor. **a**, Displacement of the antagonist ³H-*N*-methylspiperone by each of the 549 molecules tested at 10 μM. Data are mean ± s.e.m. of three assays. The molecules are coloured by their docking score. The number of molecules with substantial activity (<50% remaining radioligand, below the dashed line) diminishes with docking score. **b**, Six active compounds, each with a different scaffold. **c**, Docked poses of ZINC518842964 (left), ZINC480408888 (middle) and superposed 21433143 and 621433144 (right). The receptor helices are shown as ribbons, the conserved D115$^{3.32}$ is shown as sticks, interacting residues within 4 Å of the docked molecules are shown as lines. Ballesteros–Weinstein residue numbers are shown as superscripts. Modelled hydrogen bonds are shown as dashed lines. **d**, cAMP functional assays of the 180 pM full agonist 621433144 (orange) and the 10 nM partial agonist 464771011 (blue, agonist mode; purple, antagonist mode (464771011 and 100 nM quinpirole)). Data are mean ± s.e.m. of three assays. **e**, Gα$_{i/o}$ bioluminescence resonance energy transfer and β-arrestin-2 bioluminescence resonance energy transfer functional assays of the 180 pM full agonist 621433144 (Gα$_{i/o}$, orange; β-arrestin-2, red) and the unbiased ligand quinpirole (Gα$_{i/o}$, black; β-arrestin-2, blue). Data are mean ± s.e.m. of three assays. **f**, The effect of pre-clustering on docking scores: the orange curve is the distribution of the best-scoring scaffold representative, the blue curve is the score distribution from pre-clustering and choosing only single cluster representatives to dock.

most molecules had unconvincing receptor interactions (−43 to −35 kcal mol⁻¹). Typically, 35 to 40 molecules were tested per bin, with more in the highest scoring bins to maximize the number of active compounds found. Overall, 444 molecules were picked automatically, whereas 124 were picked by visual inspection (as described above). All molecules were tested in vitro using the same protocol.

Notably, hit rates fell almost monotonically with score, after a plateau defined by the highest-ranking molecules. In this plateau region, hit rates ranged from 22 to 26%, but below scores of −65 kcal mol⁻¹ hit rates decreased steadily to 12% for a docking score of −54 kcal mol⁻¹ and at scores of −43 kcal mol⁻¹, the hit rate reached zero, where it remained for the next two (worse) scoring bins. We fit a response curve to these observations, with a top hit rate at 24%, a bottom hit rate at 0%, a mid-point at −54 kcal mol⁻¹ and a mid-point hit-rate slope of −1.7% per kcal mol⁻¹. The regularity of this curve suggests that, at least for the D₄ receptor, ligand activity is well-predicted by docking score, notwithstanding a high false-positive rate and an inevitable false-negative rate.

From this curve we can model the total number of compounds that are active against the D₄ receptor in the library. Assuming that all molecules in a scoring range have the same hit rates, we can multiply the

total number of library molecules in any such range by the observed hit rate in that range and sum (Fig. 4). Among the library of 138 million molecules, we calculated there to be over 453,000 D₄ receptor active molecules, in over 72,600 scaffolds, with estimated K_i values of 10 μM or better (Fig. 4a, c). The number of active compounds drops to 158,000 at a more stringent 1 μM cut-off (Fig. 4b, d). Admittedly, these predictions have uncertainties, with 95% confidence intervals ranging from 188,000 to 1,035,000 active molecules and from 38,000 to 129,000 active scaffolds. Still, in some ways the estimates are conservative—for instance, we assume a 0% rate of compound discovery below a docking score of −40 kcal mol⁻¹ (Fig. 4a, b). Had we assumed a higher random hit rate, the number of discoverable compounds would have increased, as most of the library scored lower than −35 kcal mol⁻¹ (Fig. 4). Finally, we note that this unusually large set of 549 confirmed active and inactive compounds, all with docking poses, may be a useful benchmark for the field (see https://figshare.com/articles/D4_benchmark_mols_mol2/7367288/2 and Supplementary Table 4).

Human versus machine

We wondered whether molecules prioritized by docking and human visual evaluation would perform better than those prioritized
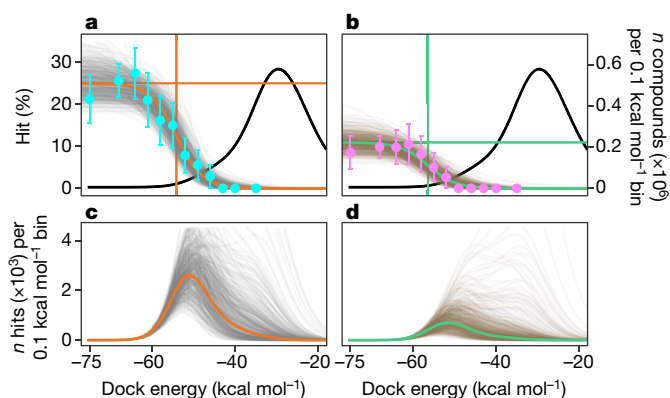
Fig. 4 | Estimating the number of active D$_4$ receptor ligands in the 138 million compound library. a, b, The hit rate of 549 tested compounds and distribution of library compounds by docking energy are shown (black curve). **a,** Modelling the number of library compounds with $K_i \leq 10\,\mu$M. The hit rate at the top plateau is 24% and at the bottom plateau is 0%, and the docking score (dock$_{50}$) and slope at the maximum (slope$_{50}$) are -54 kcal mol^{-1} and -1.7% per kcal mol^{-1}, respectively. Cyan points represent the hit rate mean $\pm$ s.e.m. at each docking energy bin, with 47, 121, 51, 38, 37, 40, 38, 36, 35, 36, 35 and 35 compounds tested in each bin, from best to worst scoring. The orange curve shows the mode and the grey curves are the draws ($n = 500$) from the Bayesian posterior distribution (that is, the envelope of possible distributions). **b,** Modelling the number of library compounds with $K_i \leq 1\,\mu$M. Top = 11%; bottom = 0%; dock$_{50}$ = -56 kcal mol^{-1}; slope = -2.8% per kcal mol^{-1}. Magenta points represent the hit rate mean $\pm$ s.e.m. at each docking energy bin. The green curve shows the mode and the brown curves show the draws from the Bayesian posterior distribution. **c, d,** Predicted number of active compounds by docking energy under the hit-rate model for the 10 μM (**c**) and 1 μM (**d**) model, with the mode (orange or green) and draws (grey or brown) from the respective posterior distributions. Expected total active compounds for the 10 μM model = 453,000 (95% interquartile range, 188,000–1,035,000) and for the 1 μM model = 158,000 (38,000–489,000).

by docking alone. From among the top 1,000 ranked molecules, we selected 124 that—on inspection—had favourable interactions, and deprioritized those with strained internal energies[30]. Another 114 high-ranking molecules were selected by docking score alone, from the same ranks. Unexpectedly, the hit rates were about the same at around 24% (Extended Data Fig. 7a). However, the molecules prioritized by human inspection typically had better affinities: 44% of these were submicromolar, which was true of only 27% of those prioritized by docking score alone. Correspondingly, a disproportionate number of the most potent agonists, such as 621433144 (180 pM) and 464771011 (14 nM), were selected by human prioritization (Extended Data Fig. 7b, c).

The docking results presented here can be compared to those from previous high-throughput screening and docking studies. For AmpC, the direct docking active 339204163 is over 20 times more potent than previously described non-covalent inhibitors[34–36], and its optimized analogue 549719643 is among the most potent non-covalent AmpC inhibitors of which we are aware. This reflects in part the simple absence of phenolates from the much smaller libraries that were previously screened. Similarly, the low- and mid-nanomolar agonists 465129598, 270269326 and 464771011 are tenfold more potent than any D$_4$ receptor screening hits of which we are aware, even from studies biased towards dopaminergic chemotypes[37], and are also more selective. Similarly, the compound 621433144 at 180 pM is among the most potent selective agonists reported for this target[38–40]. Comparing this study to a recent docking screen of 600,000 in-stock compounds against the D$_4$ receptor[14], the initial lead from the smaller library was an agonist that was effective at 260 nM, and even after three rounds of optimization resulted only in an agonist that is effective at 4 nM. As was true for the phenolate compounds that interacted with AmpC, in this case no compound that is topologically similar to 621433144 was

found in the smaller, in-stock library. It is the great expansion of the make-on-demand library, both in compounds and chemotypes, that has enabled the discovery of new ligands.

Certain caveats merit mentioning. The variation of the hit rate with docking score—although sigmoidal—was not fully monotonic, with variability among the sets of top-ranking molecules tested. Also, the estimate of active compounds is valid only for the D$_4$ receptor and has wide error margins (Fig. 4). Whereas molecules were docked as pure stereoisomers and diastereomers, they were often tested as stereochemical mixtures. Furthermore, long-standing challenges with regards to the sampling and scoring of compounds in molecular docking screens remain[41]. Whereas the hit rate versus docking score curve (Fig. 4) supports the ability to prioritize active compounds, our raw docking scores remain off-set from true binding energies, and we cannot confidently rank-order molecules for activity. Finally, docking undoubtedly continues to suffer from false-negative hits.

These caveats should not obscure our principal observations. First, docking rank predicts the likelihood that a molecule will bind to the D$_4$ receptor (Fig. 4). This suggests that docking methods[42–49], at least for well-formed binding sites, can efficiently prioritize new molecules from a large chemical space. Second, the discovery of novel and potent chemotypes for both targets suggests that the ultra-large libraries contain molecules that are better suited to a given receptor structure than can be found within the smaller in-stock libraries, and that docking can recognize them. Third, the well-behaved hit rate versus score curve (Fig. 4) allows one to predict the total number of expected active compounds for a target within a library, including those unrelated to known ligands. Integrating under this curve predicts that there are a notable 453,000 D$_4$ receptor ligands in over 72,000 scaffold families in the make-on-demand library. As daunting as these numbers are, we expect them to grow, with the library itself anticipated to exceed one billion lead-like molecules by 2020. This represents a great challenge but also a great opportunity: a 1,000-fold expansion of the molecules and chemotypes readily available to chemical biology and to drug discovery that is openly accessible to the community (http://zinc15.docking.org).

Online content

Any methods, additional references, Nature Research reporting summaries, source data, statements of data availability and associated accession codes are available at https://doi.org/10.1038/s41586-019-0917-9.

1. Bohacek, R. S., McMartin, C. & Guida, W. C. The art and practice of structure-based drug design: a molecular modeling perspective. *Med. Res. Rev.* **16**, 3–50 (1996).
2. Ertl, P. Cheminformatics analysis of organic substituents: identification of the most common substituents, calculation of substituent properties, and automatic identification of drug-like bioisosteric groups. *J. Chem. Inf. Comput. Sci.* **43**, 374–380 (2003).
3. Fink, T., Bruggesser, H. & Reymond, J. L. Virtual exploration of the small-molecule chemical universe below 160 Daltons. *Angew. Chem. Int. Ed.* **44**, 1504–1508 (2005).
4. Chevillard, F. & Kolb, P. SCUBIDOO: a large yet screenable and easily searchable database of computationally created chemical compounds optimized toward high likelihood of synthetic tractability. *J. Chem. Inf. Model.* **55**, 1824–1835 (2015).
5. Keserü, G. M. & Makara, G. M. The influence of lead discovery strategies on the properties of drug candidates. *Nat. Rev. Drug Discov.* **8**, 203–212 (2009).
6. McGovern, S. L., Caselli, E., Grigorieff, N. & Shoichet, B. K. A common mechanism underlying promiscuous inhibitors from virtual and high-throughput screening. *J. Med. Chem.* **45**, 1712–1722 (2002).
7. Brenner, S. & Lerner, R. A. Encoded combinatorial chemistry. *Proc. Natl Acad. Sci. USA* **89**, 5381–5383 (1992).
8. Ahn, S. et al. Allosteric "beta-blocker" isolated from a DNA-encoded small molecule library. *Proc. Natl Acad. Sci. USA* **114**, 1708–1713 (2017).
9. Goodnow, R. A. Jr, Dumelin, C. E. & Keefe, A. D. DNA-encoded chemistry: enabling the deeper sampling of chemical space. *Nat. Rev. Drug Discov.* **16**, 131–147 (2017).
10. Jorgensen, W. L. The many roles of computation in drug discovery. *Science* **303**, 1813–1818 (2004).
11. de Graaf, C. et al. Crystal structure-based virtual screening for fragment-like ligands of the human histamine H$_1$ receptor. *J. Med. Chem.* **54**, 8195–8206 (2011).

12. Katritch, V. et al. Structure-based discovery of novel chemotypes for adenosine A$_{2A}$ receptor antagonists. *J. Med. Chem.* **53**, 1799–1809 (2010).
13. Manglik, A. et al. Structure-based discovery of opioid analgesics with reduced side effects. *Nature* **537**, 185–190 (2016).
14. Wang, S. et al. D$_4$ dopamine receptor high-resolution structures enable the discovery of selective agonists. *Science* **358**, 381–386 (2017).
15. Negri, A. et al. Discovery of a novel selective kappa-opioid receptor agonist using crystal structure-based virtual screening. *J. Chem. Inf. Model.* **53**, 521–526 (2013).
16. Jazayeri, A., Andrews, S. P. & Marshall, F. H. Structurally enabled discovery of adenosine A$_{2A}$ receptor antagonists. *Chem. Rev.* **117**, 21–37 (2017).
17. Lane, J. R. et al. Structure-based ligand discovery targeting orthosteric and allosteric pockets of dopamine receptors. *Mol. Pharmacol.* **84**, 794–807 (2013).
18. Langmead, C. J. et al. Identification of novel adenosine A$_{2A}$ receptor antagonists by virtual screening. *J. Med. Chem.* **55**, 1904–1909 (2012).
19. Becker, O. M. et al. G protein-coupled receptors: *in silico* drug discovery in 3D. *Proc. Natl Acad. Sci. USA* **101**, 11304–11309 (2004).
20. Kooistra, A. J. et al. Function-specific virtual screening for GPCR ligands using a combined scoring method. *Sci. Rep.* **6**, 28288 (2016).
21. Congreve, M. et al. Discovery of 1,2,4-triazine derivatives as adenosine A$_{2A}$ antagonists using structure based drug design. *J. Med. Chem.* **55**, 1898–1903 (2012).
22. Kiss, R. et al. Discovery of novel human histamine H4 receptor ligands by large-scale structure-based virtual screening. *J. Med. Chem.* **51**, 3145–3153 (2008).
23. Oprea, T. I. & Gottfries, J. Chemography: the art of navigating in chemical space. *J. Comb. Chem.* **3**, 157–166 (2001).
24. Mysinger, M. M., Carchia, M., Irwin, J. J. & Shoichet, B. K. Directory of useful decoys, enhanced (DUD-E): better ligands and decoys for better benchmarking. *J. Med. Chem.* **55**, 6582–6594 (2012).
25. Bemis, G. W. & Murcko, M. A. The properties of known drugs. 1. Molecular frameworks. *J. Med. Chem.* **39**, 2887–2893 (1996).
26. Gaulton, A. et al. The ChEMBL database in 2017. *Nucleic Acids Res.* **45**, D945–D954 (2017).
27. Katz, B. A. et al. A novel serine protease inhibition motif involving a multi-centered short hydrogen bonding network at the active site. *J. Mol. Biol.* **307**, 1451–1486 (2001).
28. Congreve, M., Langmead, C. J., Mason, J. S. & Marshall, F. H. Progress in structure based drug design for G protein-coupled receptors. *J. Med. Chem.* **54**, 4283–4311 (2011).
29. Vaidehi, N. Dynamics and flexibility of G-protein-coupled receptor conformations and their relevance to drug design. *Drug Discov. Today* **15**, 951–957 (2010).
30. Irwin, J. J. & Shoichet, B. K. Docking screens for novel ligands conferring new biology. *J. Med. Chem.* **59**, 4103–4120 (2016).
31. Vass, M. et al. in *Computational Methods for GPCR Drug Discovery* (Heifetz, A.) Ch. 4, 73–113 (Humana, Springer, New Jersey, 2018).
32. Isberg, V. et al. Generic GPCR residue numbers – aligning topology maps while minding the gaps. *Trends Pharmacol. Sci.* **36**, 22–31 (2015).
33. McCorvy, J. D. et al. Structural determinants of 5-HT$_{2B}$ receptor activation and biased agonism. *Nat. Struct. Mol. Biol.* **25**, 787–796 (2018).
34. Powers, R. A., Morandi, F. & Shoichet, B. K. Structure-based discovery of a novel, noncovalent inhibitor of AmpC β-lactamase. *Structure* **10**, 1013–1023 (2002).
35. Feng, B. Y. et al. A high-throughput screen for aggregation-based inhibition in a large compound library. *J. Med. Chem.* **50**, 2385–2390 (2007).
36. Babaoglu, K. et al. Comprehensive mechanistic analysis of hits from high-throughput and docking screens against β-lactamase. *J. Med. Chem.* **51**, 2502–2511 (2008).
37. Rowley, M. et al. 5-(4-chlorophenyl)-4-methyl-3-(1-(2-phenylethyl)piperidin-4-yl)isoxazole: a potent, selective antagonist at human cloned dopamine D4 receptors. *J. Med. Chem.* **39**, 1943–1945 (1996).
38. Enguehard-Gueiffier, C. et al. 2-[(4-phenylpiperazin-1-yl)methyl]imidazo(di) azines as selective D$_4$-ligands. Induction of penile erection by 2-[4-(2-methoxyphenyl)piperazin-1-ylmethyl]imidazo[1,2-a]pyridine (PIP3EA), a potent and selective D$_4$ partial agonist. *J. Med. Chem.* **49**, 3938–3947 (2006).
39. Löber, S., Hübner, H. & Gmeiner, P. Synthesis and biological investigations of dopaminergic partial agonists preferentially recognizing the D4 receptor subtype. *Bioorg. Med. Chem. Lett.* **16**, 2955–2959 (2006).
40. Lindsley, C. W. & Hopkins, C. R. Return of D$_4$ dopamine receptor antagonists in drug discovery. *J. Med. Chem.* **60**, 7233–7243 (2017).
41. Tirado-Rives, J. & Jorgensen, W. L. Contribution of conformer focusing to the uncertainty in predicting free energies for protein-ligand binding. *J. Med. Chem.* **49**, 5880–5884 (2006).
42. Abagyan, R., Totrov, M. & Kuznetsov, D. ICM—a new method for protein modeling and design: applications to docking and structure prediction from the distorted native conformation. *J. Comput. Chem.* **15**, 488–506 (1994).
43. Halgren, T. A. et al. Glide: a new approach for rapid, accurate docking and scoring. 2. Enrichment factors in database screening. *J. Med. Chem.* **47**, 1750–1759 (2004).
44. Goodsell, D. S. & Olson, A. J. Automated docking of substrates to proteins by simulated annealing. *Proteins* **8**, 195–202 (1990).
45. Kufareva, I., Katritch, V., Stevens, R. C. & Abagyan, R. Advances in GPCR modeling evaluated by the GPCR Dock 2013 assessment: meeting new challenges. *Structure* **22**, 1120–1139 (2014).
46. Kramer, B., Rarey, M. & Lengauer, T. Evaluation of the FLEXX incremental construction algorithm for protein-ligand docking. *Proteins* **37**, 228–241 (1999).
47. McGann, M. FRED pose prediction and virtual screening accuracy. *J. Chem. Inf. Model.* **51**, 578–596 (2011).
48. Jones, G., Willett, P., Glen, R. C., Leach, A. R. & Taylor, R. Development and validation of a genetic algorithm for flexible docking. *J. Mol. Biol.* **267**, 727–748 (1997).
49. Corbeil, C. R., Williams, C. I. & Labute, P. Variability in docking success rates due to dataset preparation. *J. Comput. Aided Mol. Des.* **26**, 775–786 (2012).

Author contributions J.J.I. and B.K.S. conceived the study. J.J.I. created the enlarged docking libraries. J.L., T.E.B. and A.L. performed the docking. S.W., T.C. and B.L.R. performed D$_4$ receptor assays and analysis. I.S. performed all crystallography and assays for AmpC. Y.S.M., K.T. and A.A.T. directed the compound synthesis, purification and characterization. M.J.O. performed Bayesian modelling. E.A., T.E.B. and J.L. contributed enabling computer code. B.K.S., J.L., J.J.I., B.L.R., T.E.B., I.S., A.L., S.W., T.C. and M.J.O. wrote the paper.

METHODS

Database generation. Dockable ligand databases can be downloaded from ZINC (http://zinc15.docking.org) and protonation states and tautomers (Jchem v.15.11.23.0, https://chemaxon.com/), three-dimensional structures (Corina v.3.6.0026, https://www.mn-am.com/products/corina), conformational ensembles (omega v.2.5.1.4, https://www.eyesopen.com/omega)[50], atomic charges[51] and desolvation energies[52,53] are calculated as previously described[54]. For both the AmpC and D_4 receptor campaigns, library molecules were protonated according to experimental testing near neutral pH, using logarithmic acid dissociation constant (pK_a) values calculated according to Jchem. Whereas AmpC is known to prefer anionic molecules, and dopamine receptors are known to prefer cations, there is a precedent for uncharged molecules that bind to both[55,56]. Accordingly, the full library, unfiltered for charge state except by lead-like characteristics, was docked against both targets. The full list of docked library molecules, by ZINC number, SMILES and docking scores, has been deposited in FigShare (https://doi.org/10.6084/m9.figshare.7359626.v2 and https://doi.org/10.6084/m9.figshare.7359401.v3); from this, full charge and structural representations can be found at http://zinc15.docking.org.

Toy model for database growth. We constructed a model of ligand enrichment with library size, using the distribution of ligand and decoy docking scores. Except for the D_4 receptor, the ligands and decoys are drawn from the DUD-E benchmark; for the D_4 receptor, 48 ligands were downloaded from IUPHAR (http://www.guidetopharmacology.org) and the corresponding decoys were generated by the DUD-E web server (http://dude.docking.org/generate). Inputs to the model are the ligand-to-decoy ratio and the number of molecules in databases. From these two parameters, the distributions are sampled. We generated distributions by fitting the skewed-normal distribution to that observed for the DUD-E ligands and decoys from docking, using the statistical library in SciPy (Extended Data Fig. 1a–c and Supplementary Table 1).

Simulating hit rates from full-library docking. We docked the full make-on-demand library to investigate the ranking of ligands versus decoys. All known ligands for each target were drawn from ChEMBL[26]. Their analogues in the make-on-demand library were defined by ECFP4 Tc similarity ≥ 0.5, ≥ 0.6 or ≥ 0.7 for each target (Extended Data Fig. 1d). Together, the known active compounds and their analogues were defined as ligands, and the rest of the docked molecules were defined as decoys. The full library was then docked. To investigate the effect of library size on the ability to enrich ligands among the top 1,000 ranked compounds, 10^5, 3×10^5, 10^6, 3×10^6, 10^7, 3×10^7 and 10^8 sets of molecules were randomly selected from the full docking-ranked list and the number of ligands among the 1,000 was counted. Each set was pulled twenty times with random selection from the larger library.

Bemis–Murcko scaffold analysis. The SMILES of all the make-on-demand lead-like molecules in ZINC were downloaded from http://zinc15.docking.org/tranches/home/ on 28 February 2018. The program mitools (https://www.molinspiration.com/) calculated scaffolds for all 233 million lead-like molecules using the Bemis and Murcko method[25].

Large-scale docking. The AmpC campaign used the structure in PDB 1L2S, whereas the D_4 receptor campaign used PDB 5WIU. In each, 45 matching spheres were calculated around and including the ligand atoms—a 26 μM thiophene carboxylate for AmpC and nemonapride for D_4—and structures were prepared and AMBER united atom charges assigned[14]. The magnitude of the partial atomic charges for five residues in AmpC was increased without changing the net residue charge[55]. For both targets, the low protein dielectric was extended into the binding site using pseudo-atom positions that represented possible ligand docking sites; the radius was 1.0 Å and 2.0 Å for D_4 and AmpC, respectively[14,53,57]. For the D_4 receptor, the desolvation volume of the site was also increased by similar atom positions, using a radius of 0.3 Å. This improved the ligand charge balance in benchmarking calculations, reducing the number of high-ranking dications. Energy grids representing the AMBER van der Waals potential[58], Poisson–Boltzmann electrostatic potentials using QNIFFT[59,60] and ligand desolvation from the occluded volume of the target for different ligand orientations[53] were calculated. Using DOCK3.7.2[61], over 99 million and over 138 million library molecules were docked against AmpC and the D_4 receptor, respectively. Each library molecule was sampled in about 4,054 and 3,300 orientations and, on average, 280 and 479 conformations for AmpC and D_4, respectively, and were rigid-body-minimized with a simplex minimizer. The throughput averaged 1 s per library compound.

Clustering. To increase novelty, the high-ranking molecules from both screens were filtered for similarity to previously known ligands and for similarity to the molecules in the 3.5-million in-stock library (we have deposited tools to do this at https://github.com/docking-org/ChemInfTools). To increase diversity, the docking-ranked molecules were clustered into related families of compounds. For the AmpC screen, the top 1 million ranked molecules were best-first clustered using an ChemAxon ECFP4 Tc of 0.5 for cluster inclusion (using the Tc_c_tool that we have deposited at https://github.com/docking-org/ChemInfTools). For

the D_4 screen, we wanted to sample through the docking scoring range, and thus used a hybrid clustering approach to treat many more molecules. To cluster the 53,588,665 molecules with DOCK scores better than -30 kcal mol^{-1} against the D_4 receptor, we used best-first clustering on the first 2 million molecules (DOCK score to -49.38 kcal mol^{-1}). This resulted in 126,287 clusters. Bemis–Murcko scaffolds were calculated for the full 53,588,665 molecules, resulting in 4,893,388 scaffold-based clusters. The ECFP4-based clusters and the scaffold-based clusters were combined, and ECFP4 best-score first clustering was run on the best scoring members of each cluster, again using a 0.5 Tc cut-off. This left 423,656 hybrid clusters, each represented by its top-scoring member.

Analysis of full library docking versus pre-clustering library docking. The scaffold analysis of all docked molecules against AmpC and D_4 receptor used Bemis–Murcko scaffolds, as above. For the full library docking, the best-scoring member was selected to represent the scaffold. To investigate the influence of only docking cluster representatives, rather than docking the full library, scaffold representatives were picked by four different methods: (1) the closest member to the centroid by molecular mass and a calculated log octanol/water value of the partition coefficient of the compound (clogP), (2) the closest member to the centroid of molecular mass alone, (3) the member with the largest molecular mass and (4) the member with the smallest molecular mass. The molecular mass values are calculated and the clogP values are predicted by Rdkit (http://www.rdkit.org).

Analoging within the library. The 90 AmpC analogues from within the make-on-demand library were selected on the basis of topological similarity to the primary docking hits: each had an ECFP4-based Tc ≥ 0.5 or shared the same substructure as the initial hit. All prioritized analogues also had favourable docking scores to the enzyme.

Make-on-demand synthesis. Compounds were synthesized using 70,000 qualified in-stock building blocks and 130 well-characterized, two-component reactions at Enamine. Historically, molecules have been synthesized in three to four weeks with an 85% fulfilment rate; in this project delivery time was six weeks, but with a 93% fulfilment rate. Each reaction is well-tested for conditions, including temperatures, completion time and mixing, as previously described[62]. Typically, compounds are made in parallel by combining reagents and solvents in a single vial in the appropriate conditions to allow the reaction to proceed to completion. The product-containing vial is filtered by centrifugation into a second vial to remove precipitate and the solvent is evaporated under reduced pressure; the product is then purified by high-performance liquid chromatography. Identity and purity is assessed by liquid chromatography–mass spectrometry, ^{1}H and ^{13}C NMR. All compounds were shipped with 90% (most with 95%) or higher purity (Supplementary Tables 9, 10 and Supplementary Data 11–14).

AmpC crystallography. All four inhibitors, 547933290, 275579920, 339204163 and 549719643, were cocrystallized from 1.7 M potassium phosphate with microseeding at pH values that varied from 8.7 to 8.9, as previously described[63]. Crystals were cryo-cooled in a solution that contained a reservoir solution and 25% sucrose. Reflections were measured at beamline 8.3.1 of the Advanced Light Source with a wavelength of 1.11583 nm at a temperature of 100 K. Complexes with 547933290, 275579920, 339204163 and 549719643 were measured to a resolution of 1.50 Å, 1.91 Å, 1.90 Å and 1.79 Å, respectively (Extended Data Table 1). All four complexes crystallized in the C2 space group with two molecules in the asymmetric unit[63]. The datasets were indexed, scaled and merged using XDS and AIMLESS[64]. MOLREP was used for molecular replacement using the protein model from PDB 1KE4, giving unbiased electron densities for the inhibitor in initial electron density maps. Initial model fitting and water addition was done in COOT[65] followed by refinement in REFMAC[66]. Geometry restraints of inhibitor molecules were created in eLBOW-PHENIX. Following inhibitor modelling in COOT, refinement was carried out using PHENIX[67]. For each structure, geometry was assessed using MolProbity. The final models of 547933290, 275579920, 339204163 and 549719643 in complex with AmpC were refined to R_{work} and R_{free} values of 19.1 and 22.3%, 19.4 and 23.2%, 17.1 and 20.3%, and 18.6 and 22%, respectively. Coordinates have been deposited with PDB identifiers 6DPZ, 6DPY, 6DPX and 6DPT, respectively. Model quality was confirmed using PROCHECK. The total number of residues located in the most favourable and allowed region of the Ramachandran plot for the complexes with 547933290, 275579920, 339204163 and 549719643 were 97.89% and 2.11%, 98.03% and 1.97%, 98.31% and 1.69%, and 98.03% and 1.97%, respectively. The data measurement and refinement statistics are summarized in Extended Data Table 1.

AmpC enzymology. All candidate inhibitors were dissolved in DMSO at 30 mM, and more dilute DMSO stocks were prepared as necessary so that the concentration of DMSO was held constant at 1% v/v in 50 mM sodium cacodylate buffer, pH 6.5. AmpC activity and inhibition was monitored spectrophotometrically using either CENTA or nitrocephin as substrates[68]. All assays included 0.01% Triton X-100 to reduce compound aggregation artefacts[69]. Active compounds were further investigated for aggregation by dynamic light scattering and by inhibition of three counter-screening enzymes: trypsin, chymotrypsin and malate dehydrogenase[36].

Unless otherwise stated, no active compound was found to form aggregates nor did they inhibit any of the three counter-screening enzymes (Supplementary Tables 2, 3). IC_{50} values reflect the percentage inhibition fit to a dose–response equation in GraphPad Prism (GraphPad), whereas K_i values were calculated directly from Lineweaver–Burk plots for all compounds, except for ZINC170811339, ZINC184991516, ZINC171610178 and 547933290, for which the Cheng–Prusoff equation was used.

D_4 receptor radioligand binding assay. Binding was measured using membrane preparations from HEK293T cells that transiently expressed human D_2 (D_2 long receptor), D_3 and D_4 ($D_{4.4}$ variant). HEK293T cells (ATCC CRL-11268; 59587035; mycoplasma free) were transfected and membrane preparation and radioligand binding assays were set up in 96-well plates in the standard binding buffer (50 mM Tris, 10 mM $MgCl_2$, 0.1 mM EDTA, 0.1% BSA, pH 7.4)[14]. For primary screening, 10 μM compounds were incubated with membrane and radioligands (0.8–1.0 nM ^3H-N-methylspiperone) (PerkinElmer). For displacement experiments, test compounds with increasing concentrations were incubated with the membrane and radioligands (0.8–1.0 nM ^3H-N-methylspiperone). Reactions for either primary screening or displacement experiments were incubated for 2 h at room temperature in the dark and terminated by rapid vacuum filtration onto chilled 0.3% PEI-soaked GF/A filters, followed by three quick washes with cold washing buffer (50 mM Tris HCl, pH 7.4) and quantified as previously described[70]. Results (with or without normalization) were analysed using GraphPad Prism 5.0 using one-site shift models where indicated.

cAMP inhibition assay. To measure D_4 $G\alpha_{i/o}$-mediated cAMP inhibition, HEK293T (ATCC CRL-11268; 59587035; mycoplasma free) cells were co-transfected with human D_4 ($D_{4.4}$ variant) along with a luciferase-based cAMP biosensor (GloSensor; Promega) and assays were performed as previously described[14]. After 16 h, transfected cells were seeded in poly-L-lysine-coated 384-well white clear-bottom cell culture plates (Greiner; 10,000 cells per well, 40 μl per well) in DMEM containing 1% dialysed FBS. The next day, ligand solutions were prepared in fresh buffer (20 mM HEPES, 1× HBSS, 0.3% bovine serum album (BSA), pH 7.4) at 3× the drug concentration. Plates were decanted and received 20 μl per well of ligand buffer followed by addition of 10 μl of ligand solution (3 wells per condition) for 15 min in the dark at room temperature. To measure agonist activity for $G\alpha_{i/o}$-coupled receptors, 10 μl luciferin (4 mM final concentration) supplemented with isoproterenol (400 nM final concentration was added to activate G_s via endogenous β_2-adrenergic receptors) and luminescence intensity was quantified 10 min later. Data were analysed using 'log(agonist) versus response' in GraphPad Prism 5.0.

Bioluminescence resonance energy transfer (BRET) assay. To measure D_4-mediated G protein activation, HEK293T cells were co-transfected with human D_4, $G\alpha_i1$ containing C-terminal *Renilla* luciferase (RLuc8), $G\beta$ and $G\gamma$ containing a C-terminal GFP (at mass ratio 1:0.3:2:2, respectively). To measure D_4-mediated arrestin recruitment, HEK293T cells were co-transfected with human D_4 containing C-terminal RLuc8 and β-arrestin-2 containing a N-terminal YFP at ratio 1:3. After at least 16 h, transfected cells were plated in poly-L-lysine-coated 96-well white clear-bottom cell culture plates in plating medium (DMEM and 1% dialysed FBS) at a density of 40,000–50,000 cells in 200 μl per well and incubated overnight. The next day, the medium was decanted and cells were washed twice with 60 μl of drug buffer (20 mM HEPES, 1× HBSS, pH 7.4), then 60 μl of the RLuc substrate, coelenterazine 400a for G protein assay, and coelenterazine h for β-arrestin-2 assay (Promega, 5 μM final concentration in drug buffer), was added per well, incubated an additional 5 min to allow for substrate diffusion. Afterwards, 30 μl of drug (3×) in drug buffer (20 mM HEPES, 1× HBSS, 0.1% BSA, pH 7.4) was added per well and incubated for another 5 min. Plates were immediately read for luminescence at 400 nm and GFP fluorescence emission at 515 nm (G protein assay); 485 nm and eYFP fluorescence emission at 530 nm (β-arrestin-2 assay) for 1 s per well using a Mithras LB940 multimode microplate reader. The ratio of GFP/RLuc or eYFP/RLuc was calculated per well and the net BRET ratio was calculated by subtracting the GFP/RLuc or eYFP/RLuc from the same ratio in wells without GFP or eYFP present. The net BRET ratio was plotted as a function of drug concentration using Graphpad Prism 5 (Graphpad).

Hit-rate curve prediction and estimation of maximum number of hits. To define the docking scoring ranges from which molecules would be picked for experimental testing, we used distributions of prior probabilities from Bayesian statistics for highest, mid-point and random hit rates, and for the slope of the curve. To advance the argument, we assumed that docking hit rates would behave in a manner similar to a dose–response curve as a function of docking energy, e_i:

$$\text{HitRate}(e_i) = \frac{\text{top} - \text{bottom}}{1 - e^{-S \cdot (e_i - \text{dock}_{50})}} + \text{bottom}$$

This function is defined by four parameters: (1) top is the maximum hit rate; (2) dock_{50} is the dock energy in kcal mol^{-1} at top/2; (3) $S = \text{slope} \times 4/\text{top}$, in which slope

is the change in the hit rate at dock_{50} in hit rate %/(kcal mol^{-1}); and (4) bottom is the minimum hit rate that we fixed at zero. To define the prior probability distribution, 4 authors graded 440 compounds across 11 energy slices (Extended Data Fig. 8e), from which we chose independent Bayesian prior probabilities for each parameter, $P(\text{top}) = \text{beta}(\alpha = 20, \beta = 80)$, $P(\text{dock}_{50}) = \text{normal}(\mu = -60, \sigma = 15)$, $P(S) = \text{normal}(\mu = -0.2, \sigma = 0.1)$ (Extended Data Fig. 8b–d). To sample curves from the posterior distribution given the prior distribution and given the results of testing the 549 compounds, we used Hamiltonian Monte Carlo with no-u-turn sampling with Stan[71] (four chains of 50,000 warm-up and 50,000 sampling steps each and adapt_delta = 0.99 and max_treedepth = 12 control parameters) (Fig. 4a and Extended Data Fig. 8b–d). To select the most informative compounds to test, we evaluated the Shannon information gain of six candidate designs, defined as the expected difference in posterior minus prior entropy over the prior-predictive distribution, by nested Monte Carlo[72,73]. We selected design 5 favouring higher information gain over number of active compounds (Extended Data Fig. 8f). To estimate the number of active compounds (Fig. 4b) and scaffolds (Extended Data Fig. 8g), the energies of the compounds and scaffold cluster heads were integrated over the uncertainty in the posterior hit-rate model (Extended Data Fig. 8h, i).

Code availability. DOCK3.7 is freely available for non-commercial research http://dock.compbio.ucsf.edu/DOCK3.7/. A web-based version is available at http://blaster.docking.org/.

Reporting Summary. Further information on research design is available in the Nature Research Reporting Summary linked to this article.

Data availability

Active molecules reported here are available from B.K.S. or directly from Enamine. The four structures of AmpC determined with the new docking hits are available from the PDB with accession numbers 6DPZ, 6DPY, 6DPX and 6DPT. The compounds docked in this study are freely available from our ZINC lead-like make-on-demand library (http://zinc15.docking.org). All active compounds are available either from the authors or may be purchased from Enamine. Figures with associated raw data include: Fig. 2, for which electron density and reflection files are deposited with the PDB; Figs. 3, 4 and Extended Data Fig. 5, for which Source Data are available in the online version of the paper; Extended Data Fig. 1, for which the data are included in Supplementary Table 1; Extended Data Fig. 6, for which raw clustering or no-clustering rank numbers are included in Supplementary Tables 8, 9. Further data are provided in Supplementary Tables 3, 5 (aggregation assays for AmpC inhibitors and D_4 ligands); Extended Data Table 1 (crystallographic data collection and refinement); Supplementary Tables 9, 10 and Supplementary Data 12–15 (chemical purity of active ligands and their spectra); Supplementary Data 11 and 14 (synthetic routes to compounds). All other data are available from the authors on request.

50. Hawkins, P. C., Skillman, A. G., Warren, G. L., Ellingson, B. A. & Stahl, M. T. Conformer generation with OMEGA: algorithm and validation using high quality structures from the Protein Databank and Cambridge Structural Database. *J. Chem. Inf. Model.* **50**, 572–584 (2010).
51. Hawkins, G. D. et al. AMSOL version 7.1 https://comp.chem.umn.edu/amsol/ (2004).
52. Wei, B. Q., Baase, W. A., Weaver, L. H., Matthews, B. W. & Shoichet, B. K. A model binding site for testing scoring functions in molecular docking. *J. Mol. Biol.* **322**, 339–355 (2002).
53. Mysinger, M. M. & Shoichet, B. K. Rapid context-dependent ligand desolvation in molecular docking. *J. Chem. Inf. Model.* **50**, 1561–1573 (2010).
54. Sterling, T. & Irwin, J. J. ZINC 15—ligand discovery for everyone. *J. Chem. Inf. Model.* **55**, 2324–2337 (2015).
55. Barelier, S. et al. Increasing chemical space coverage by combining empirical and computational fragment screens. *ACS Chem. Biol.* **9**, 1528–1535 (2014).
56. Gray, D. L. et al. Impaired β-arrestin recruitment and reduced desensitization by non-catechol agonists of the D1 dopamine receptor. *Nat. Commun.* **9**, 674 (2018).
57. Carlsson, J. et al. Ligand discovery from a dopamine D_3 receptor homology model and crystal structure. *Nat. Chem. Biol.* **7**, 769–778 (2011).
58. Meng, E. C., Shoichet, B. K. & Kuntz, I. D. Automated docking with gridb-based energy evaluation. *J. Comput. Chem.* **13**, 505–524 (1992).
59. Sharp, K. A., Friedman, R. A., Misra, V., Hecht, J. & Honig, B. Salt effects on polyelectrolyte-ligand binding: comparison of Poisson–Boltzmann, and limiting law/counterion binding models. *Biopolymers* **36**, 245–262 (1995).
60. Gallagher, K. & Sharp, K. Electrostatic contributions to heat capacity changes of DNA-ligand binding. *Biophys. J.* **75**, 769–776 (1998).
61. Coleman, R. G., Carchia, M., Sterling, T., Irwin, J. J. & Shoichet, B. K. Ligand pose and orientational sampling in molecular docking. *PLoS ONE* **8**, e75992 (2013).
62. Tolmachev, A. et al. Expanding synthesizable space of disubstituted 1,2,4-oxadiazoles. *ACS Comb. Sci.* **18**, 616–624 (2016).
63. Eidam, O. et al. Design, synthesis, crystal structures, and antimicrobial activity of sulfonamide boronic acids as β-lactamase inhibitors. *J. Med. Chem.* **53**, 7852–7863 (2010).
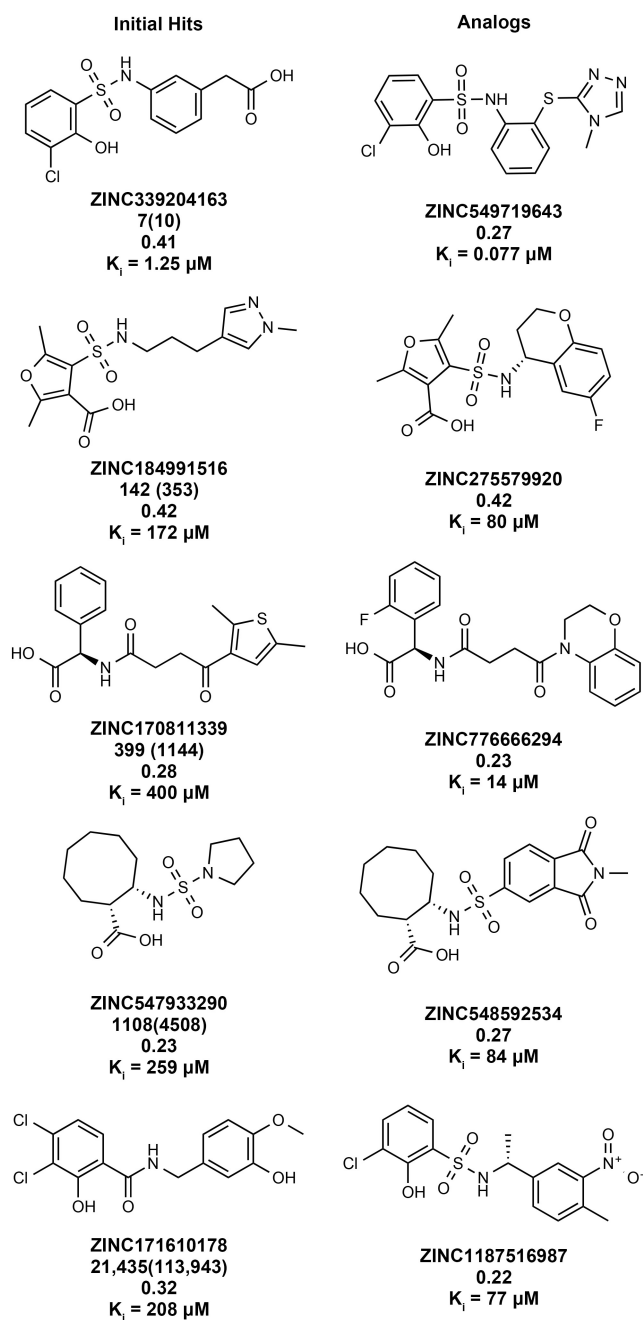64. Kabsch, W. XDS. *Acta Crystallogr. D* **66**, 125–132 (2010).

65. Emsley, P., Lohkamp, B., Scott, W. G. & Cowtan, K. Features and development of Coot. *Acta Crystallogr. D* **66**, 486–501 (2010).
66. Murshudov, G. N., Vagin, A. A. & Dodson, E. J. Refinement of macromolecular structures by the maximum-likelihood method. *Acta Crystallogr. D* **53**, 240–255 (1997).
67. Adams, P. D. et al. PHENIX: a comprehensive Python-based system for macromolecular structure solution. *Acta Crystallogr. D* **66**, 213–221 (2010).
68. Eidam, O. et al. Fragment-guided design of subnanomolar β-lactamase inhibitors active in vivo. *Proc. Natl Acad. Sci. USA* **109**, 17448–17453 (2012).
69. Feng, B. Y. & Shoichet, B. K. A detergent-based assay for the detection of promiscuous inhibitors. *Nat. Protoc.* **1**, 550–553 (2006).
70. Allen, J. A. et al. Discovery of β-arrestin-biased dopamine D_2 ligands for probing signal transduction pathways essential for antipsychotic efficacy. *Proc. Natl Acad. Sci. USA* **108**, 18488–18493 (2011).
71. Carpenter, B. et al. Stan: a probabilistic programming language. *J. Stat. Softw.* **1**, 1–32 (2017).
72. Ryan, E. G., Drovandi, C. C., McGree, J. M. & Pettitt, A. N. A review of modern computational algorithms for Bayesian optimal design. *Int. Stat. Rev.* **84**, 128–154 (2016).
73. Rainforth, T., Cornish, R., Yang, H., Warrington, A. & Wood, F. On Nesting Monte Carlo Estimators. In *Proc. 35th International Conference on Machine Learning PMLR* 80 (eds Dy, J. & Krause, A.) 4267–4276 (2018).
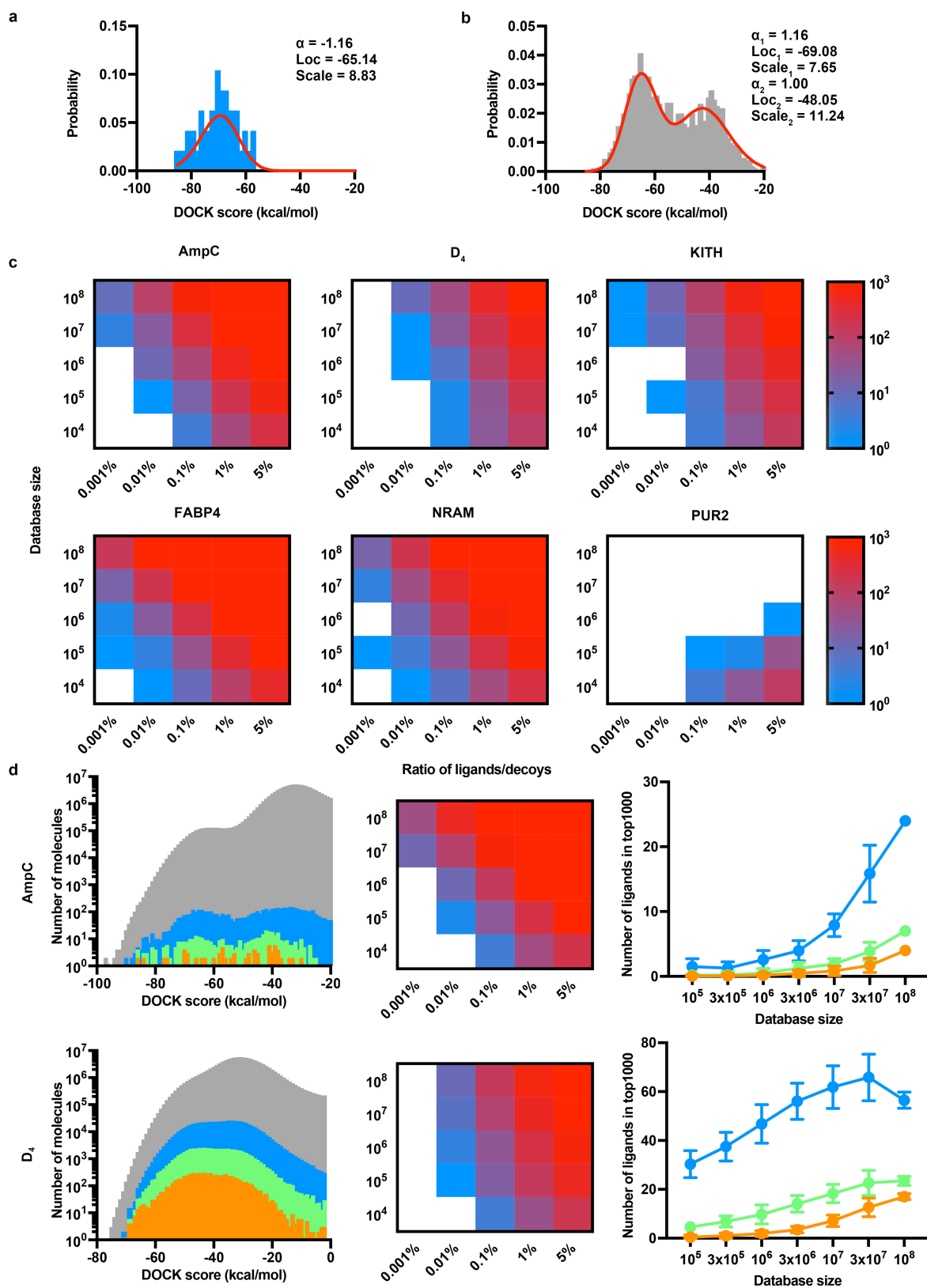
Extended Data Fig. 1 | See next page for caption.

Extended Data Fig. 1 | Simulating the effect of library size on ligand enrichment among the top 1,000 docked molecules. a, **b**, The energy distribution of ligands (**a**) and decoys (**b**) from docking enrichment calculations against AmpC. The skewed normal fitting curves are plotted in red lines. The fitting parameters (shape (α), location (loc) and scale values) are shown. **c**, Heat maps of the number of active molecules in the top 1,000 docked molecules for 6 targets. The number of ligands in the top 1,000 docked molecules for a given library size and the ratio between ligands and decoys is coloured using a $\log_{10}$(number of ligands) scale ranging from 1 (blue) to 1,000 (red). Cells with zero ligands are shown in white. **d**, Large-library docking screens of AmpC (top, $n = 99$ million molecules) and D_4 (bottom, $n = 138$ million molecules). Molecules

that are known to bind to AmpC and D_4, as well as close analogues, are treated as ligands and the rest of the molecules are treated as decoys. Left, the energy distributions of decoys (grey), ligands defined by ECFP4 Tc similarity ≥ 0.5 (blue), 0.6 (green) and 0.7 (orange) to ligands from ChEMBL. Middle, heat maps of the number of ligands in the top 1,000 docked molecules based on fit to full-library docking with the ligands (AmpC, Tc ≥ 0.5, green; D_4, Tc ≥ 0.6, orange) and decoys (grey) distributions. Right, number of ligands in the top 1,000 docked molecules as the library grows based on actual distributions plotted in the left panel. Data are mean $\pm$ s.d. of 20 samples. See Supplementary Table 1 for retrospective performance on three more targets.

Initial Hits   Analogs

ZINC339204163
7(10)
0.41
K_i = 1.25 µM

ZINC549719643
0.27
K_i = 0.077 µM

ZINC184991516
142 (353)
0.42
K_i = 172 µM

ZINC275579920
0.42
K_i = 80 µM

ZINC170811339
399 (1144)
0.28
K_i = 400 µM

ZINC776666294
0.23
K_i = 14 µM

ZINC547933290
1108(4508)
0.23
K_i = 259 µM

ZINC548592534
0.27
K_i = 84 µM

ZINC171610178
21,435(113,943)
0.32
K_i = 208 µM

**ZINC1187516987**
0.22
K_i = 77 µM

Extended Data Fig. 2 | Initial hits and selected analogues against AmpC. The five initial hits are shown in the left column. Under each compound, the first row includes the ZINC identifier; the second row is the cluster rank (position in cluster head list sorted by DOCK score) with global rank (position in unclustered hit list sorted by DOCK score) shown in brackets; the third row is the Tc value (Tanimoto coefficient to known AmpC inhibitors in ChEMBL); the fourth row is the K_i value. Five selected analogues for the corresponding hits are shown in the right column. Under each compound, the first row includes the ZINC identifier; the second row is the Tc value; and the third row is the K_i value.
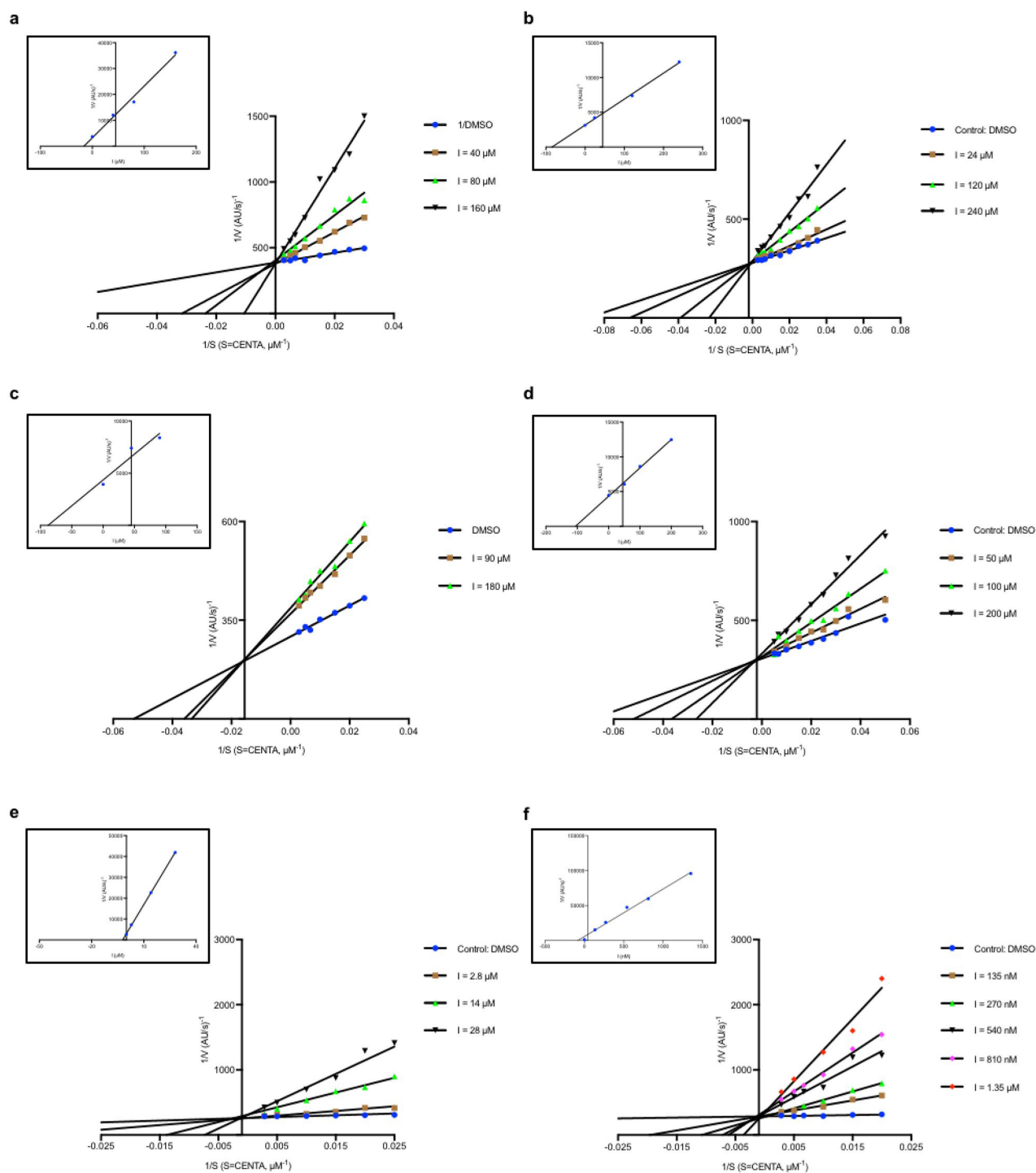
Extended Data Fig. 3 | Lineweaver–Burk plot and K_i analysis for analogues of each of the five series of AmpC inhibitors. **a–f**, Lineweaver–Burk plots for ZINC776666294 (**a**), 275579920 (**b**), ZINC548592534 (**c**), ZINC1187516987 (**d**), 339204163 (**e**) and 549719643 (**f**), indicating competitive inhibition. IC$_{50}$ values were determined by nonlinear regression fit in GraphPad Prism, and K_i values calculated by a replot of the slope of each Lineweaver–Burk plot versus the corresponding inhibitor concentration.
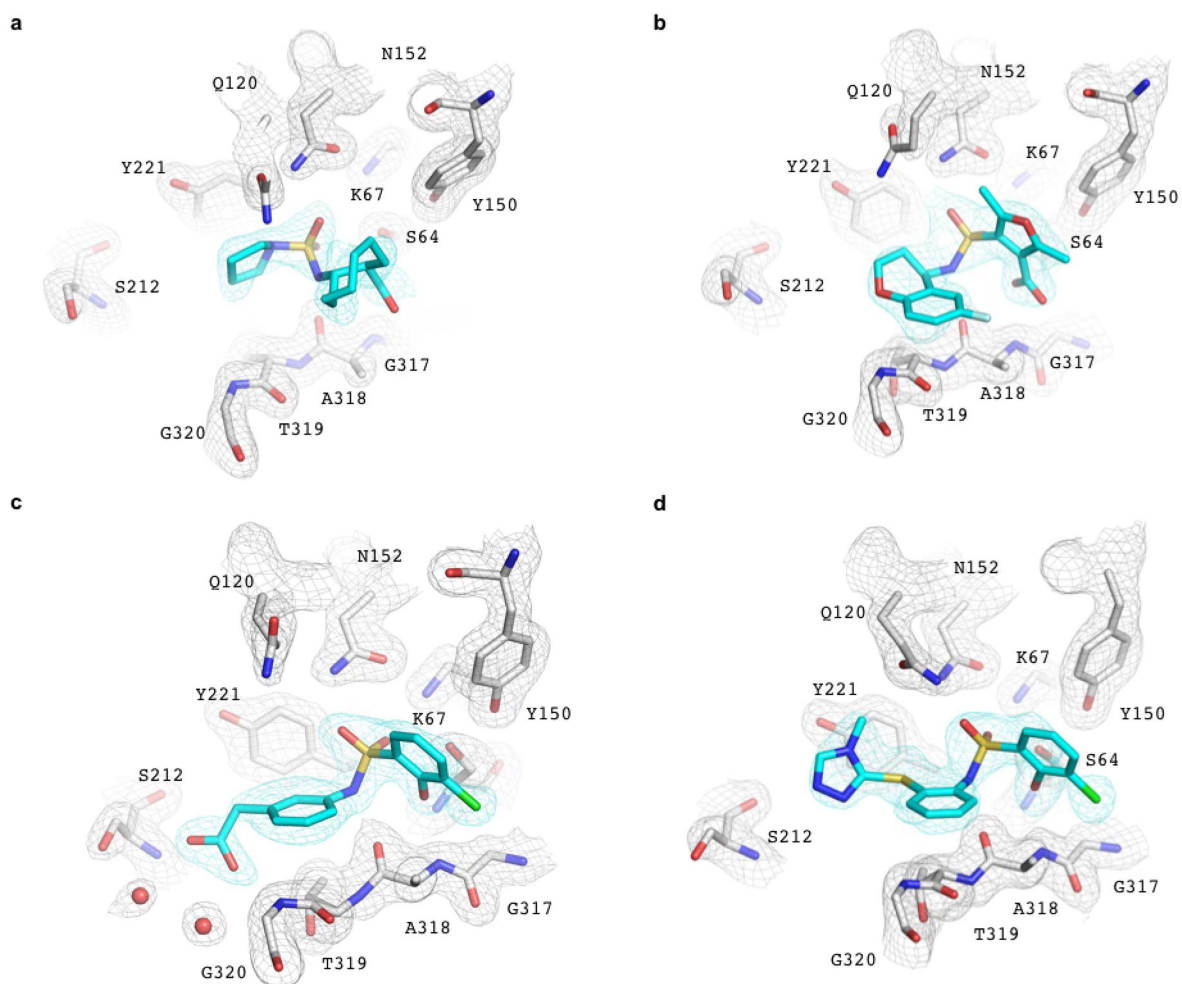
Extended Data Fig. 4 | Electron density maps for AmpC–inhibitor complexes. The initial $F_o - F_c$ electron density map contoured at 2.5σ around the inhibitor (density in cyan) with refined $2F_o - F_c$ electron density contoured at 1σ for enzyme residues for the complexes with the following compounds. **a**, 547933290. **b**, 275579920. **c**, 339204163. **d**, 549719643. Inhibitor carbons are shown in cyan and enzyme carbons are shown in grey, oxygens in red, nitrogens in blue, sulfurs in yellow and chlorides in green.
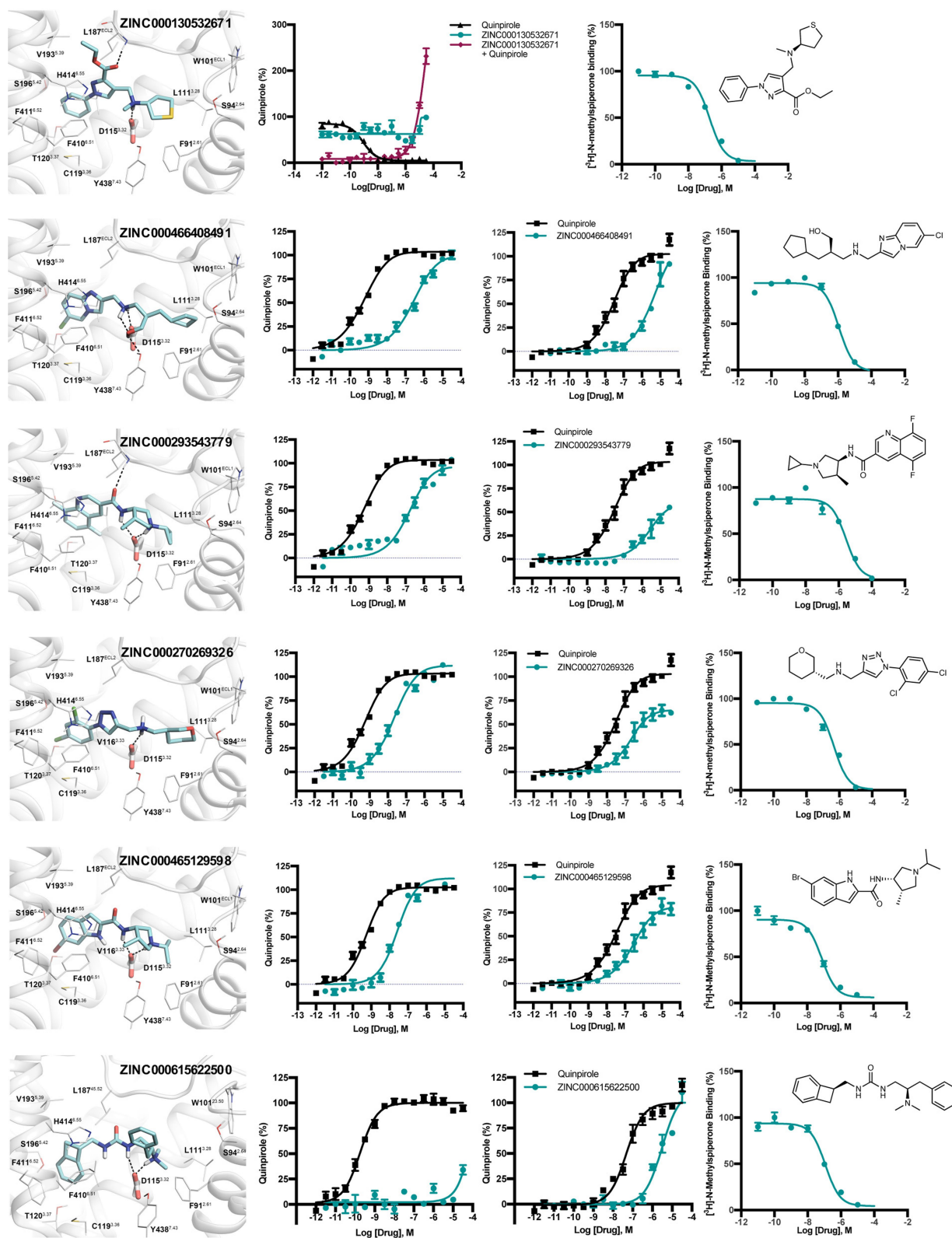
Extended Data Fig. 5 | Selected D_4 hits from docking 138 million make-on-demand molecules. Six ligands with docked poses (first column), cAMP $G\alpha_{i/o}$ activities (second column), Tango β-arrestin activities (third column) and ^{3}H-N-methylspiperone displacement and chemical drawing (fourth column) are shown. The receptor structure is in grey and ligand carbons are in teal. Ballesteros–Weinstein residue numbers are included as superscripts. Functional assays represent normalized concentration–response curves of the ligands in cloned human D_4-mediated activation of $G\alpha_{i/o}$ and β-arrestin translocation. Data are mean $\pm$ s.e.m. of three assays. The first row shows an example of an antagonist identified among the D_4 hits. Both agonist (teal curve) and antagonist (purple curve) modes are shown for ZINC130532671 in the third panel; the concentration of quinpirole in the antagonist mode was 100 nM.
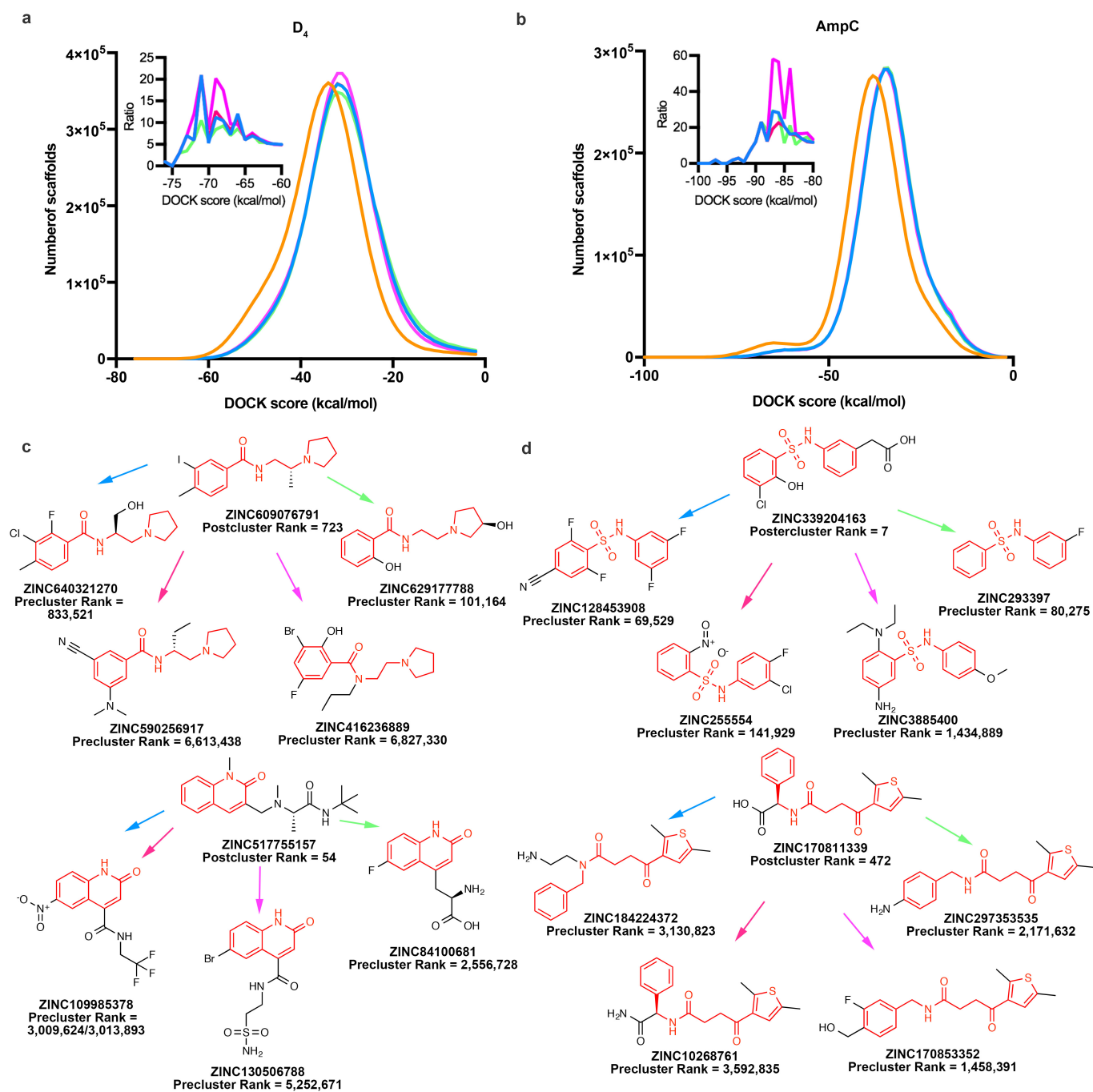
Extended Data Fig. 6 | Pre-clustering the docking library yields much worse scores of scaffold representatives compared to full library docking. a, b, Comparison of energy distributions of scaffold representatives between full library docking (orange) and pre-clustered library docking for D_4 (**a**) and AmpC (**b**) using four strategies: the closest member to the centroid of molecular masses and clog$P$ (blue), the closest member to the centroid of molecular masses (pink), the member with the largest molecular masses (magenta) and the member with the smallest molecular masses (green). The inset shows the ratio of the number of molecules at a given docking score for full library docking divided by the number at that score when only cluster representatives are docked (coloured by clustering method). For each target, two examples illustrate the effect on our experimentally active scaffold families. **c,** D_4. **d,** AmpC. The scaffold for each molecule is highlighted in red. The ZINC identifier, post-cluster rank and pre-cluster rank are labelled for each pair. The arrow colour is as for the pre-clustering methods in **a** and **b**.
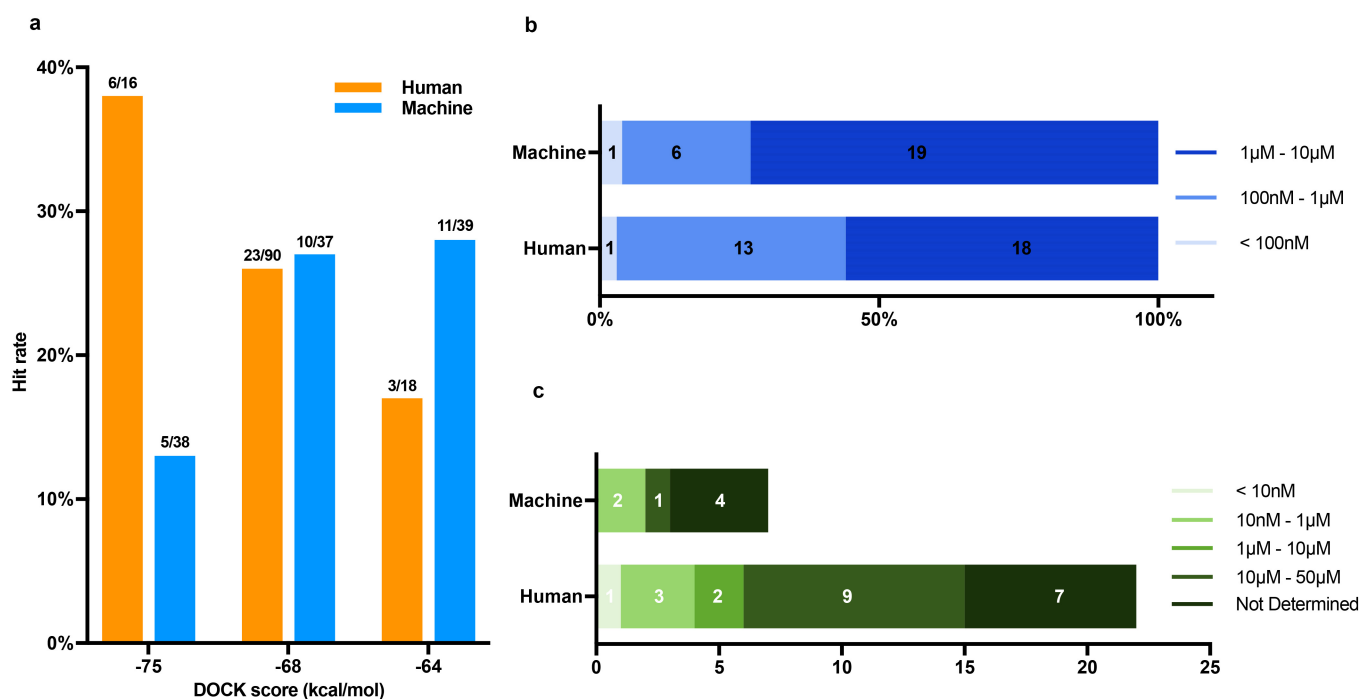
Extended Data Fig. 7 | Comparison of hit rates achieved by combined docking score and human prioritization compared to the rates achieved by docking score alone. a, The hit rates for selecting compounds at different scoring ranges by each strategy: human prioritization and docking score (orange), or docking score alone (blue). Hit rate is the ratio of active compounds/tested compounds; the raw numbers appear at the top of each bar. **b,** Distribution of the binding affinity level among the hits from **a**. There are 32 hits from human prioritization and docking score, and 26 hits from the docking score alone. These are divided into three affinity ranges: <100 nM (pale blue); 100 nM–1 μM (blue); 1–10 μM (dark blue). **c,** Functional activity distribution among the hits from **b**. There are 22 molecules from human prioritization and docking score, and 7 molecules from the docking score alone. These are divided into five activity ranges: <10 nM (pale green); 10 nM–1 μM (light green); 1–10 μM (olive); 10–50 μM (forest green); and not determined (dark green).
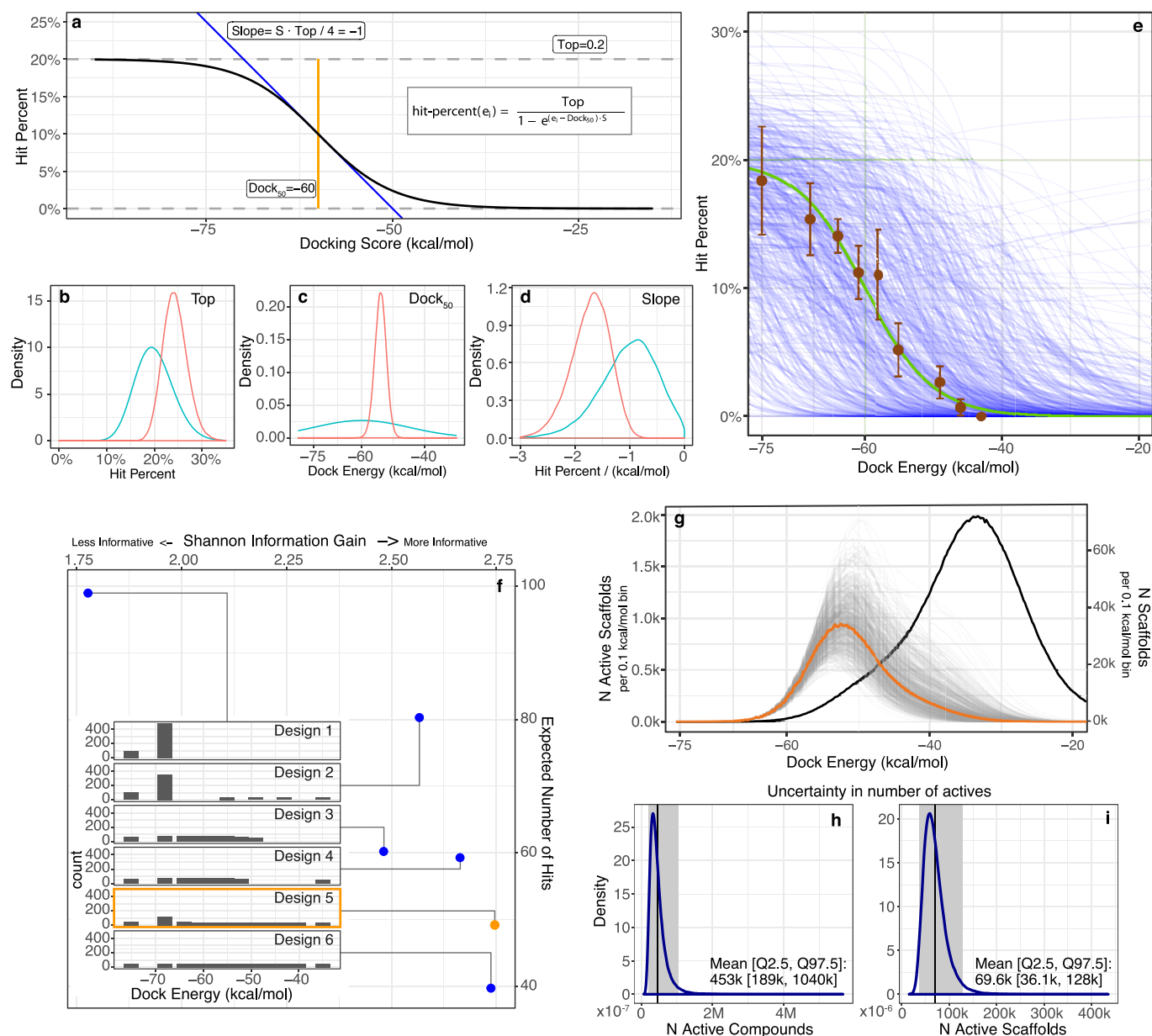
Extended Data Fig. 8 | Bayesian prior modelling for balancing information gain and ligand discovery in molecule-selection design and error estimation. a, Sigmoid functional form for the hit-rate model. **b–d**, Marginal Bayesian prior (teal) and posterior (red) distributions ($n = 200{,}000$) for each model parameter. **b**, Top. **c**, Dock$_{50}$. **d**, Slope. **e**, Estimated hit rate based on evaluation by the authors of the docked poses before any molecules were tested. Brown, mean $\pm$ s.d.; $n = 200, 220, 230,$ 230, 285, 235, 210, 230 and 200 compounds; $n = 5, 4, 4, 4, 4, 4, 4, 4$ and

4 experts. The prior mean (green) and samples ($n = 200$) from the prior (blue) are shown. **f**, Candidate (blue) and chosen (orange) experimental designs (inset, designs 1–6), with expected number of hits and information gain for each design. **g**, Expected number of active scaffolds (orange, mean; grey, posterior draws $n = 200{,}000$) superimposed on the total number of scaffold cluster heads (black). **h, i**, Marginal distribution of the number of active compounds (**h**) and scaffolds (**i**) over the posterior distributions ($n = 200{,}000$).

Extended Data Table 1 | Data collection and refinement statistics of AmpC inhibitors

		ZINC547933290	ZINC275579920	ZINC339204163	ZINC549719643
Data collection					
Space group		C2	C2	C2	C2
Cell dimensions					
	a, b, c (Å)	97.70, 77.73, 115.68	97.44, 77.56, 118.41	98.02, 77.7, 115.94	98.17, 77.56, 115.51
	a, b, g (°)	90.00, 113.26, 90.00	90.00, 116.05, 90.00	90.00, 113.35, 90.00	90.00, 113.04, 90.00
Resolution (Å)		62.75-1.50 (1.53-1.50) *	62.67-1.91 (1.95-1.91)	62.76-1.90 (1.94-1.90)	87.87-1.79 (1.83-1.79)
R_{sym} or R_{merge}		5.6 (17.1)	14 (20.7)	5.3 (35)	6.9 (10.9)
I / sI		13.6 (1.0)	10 (1.1)	19.6 (4.3)	13.5 (1.7)
Completeness (%)		99.5 (98.6)	97.4 (96)	96.4 (71.1)	99.8 (99.6)
Redundancy		6.6 (6.4)	6.9 (7.1)	6.4 (5.0)	6.6 (6.0)
Refinement					
Resolution (Å)		62.7-1.5	58.64-1.91	45.8-1.90	58.46-1.79
No. reflections		126186	59879	60717	74953
R_{work} / R_{free}		19.2/22.3	19.5/23.2	17.2/20.2	18.8/21.9
No. atoms					
	Protein	5499	5483	5513	5499
	Ligand/ion	40	50	44	50
	Water	593	237	326	269
B-factors					
	Protein	29.34	33.09	29.76	34.57
	Ligand/ion	35.14	38.60	36.59	42.63
	Water	37.86	35.87	34.59	38.55
R.m.s. deviations					
	Bond lengths (Å)	0.007	0.007	0.008	0.007
	Bond angles (°)	0.86	0.84	0.86	0.85

One crystal for each structure was used.
*Values in parentheses are for the highest-resolution shell.

Extended Data Table 2 | The highest-affinity direct docking hits for the D$_4$ receptor

ZINC ID	Cluster Rank*	Tc†	cAMP EC$_{50}$ (nM)	G$_i$ BRET EC$_{50}$ (nM)	Tango EC$_{50}$ (nM)	Arrestin BRET EC$_{50}$ (nM)	Bias Factor	K$_i$ (nM)		
								D$_4$	D$_2$	D$_3$
ZINC621433144	611	0.33	0.18	0.56	57.3	2.3	17 to G protein	4.30	>10,000	>10,000
ZINC621433143 (diastereomeric mixture)	611	0.33	2.3	22.8	74.1	13.03	1	18	>10,000	>10,000
ZINC361131264	611	0.33	7.3	21.93	151	890.1	26 to G protein	72	>10,000	>10,000
ZINC361131265	611	0.33	59	1,778	556	ND‡	11 to G protein	185	>10,000	>10,000
ZINC621433143	611	0.33	350	3,148	898	1,246	7 to Arrestin	669	>10,000	>10,000
ZINC464771011	937	0.32	10.4	NT§	1,141	NT	3 to Arrestin	140	>10,000	>10,000
ZINC270269326	1,510	0.32	17	11.7	172.3	NT	2 to Arrestin	500	>10,000	>10,000
ZINC465129598	1,565	0.32	24	22.9	210.1	NT	2 to Arrestin	80	>10,000	>10,000
ZINC278933042	5,796	0.27	41	NT	22,340	NT	NT	270	>10,000	>10,000
ZINC293543779	420	0.31	130	NT	1,684	NT	1	1200	>10,000	>10,000
ZINC466408491	274	0.27	270	NT	8,529	NT	4 to Arrestin	3,900	4,780	5,430
ZINC567992445	5,854	0.33	4,820	NT	NT	NT	NT	850	>10,000	>10,000
ZINC413570733	81,969	0.28	IC$_{50}$ = 5,900	NT	NT	NT	NT	130	>10,000	>10,000
ZINC155719879	132	0.31	7,200	NT	NT	NT	NT	460	>10,000	>10,000
ZINC569686370	17,659	0.34	7,800	NT	NT	NT	NT	550	>10,000	>10,000
ZINC268141382	734	0.3	9,900	NT	NT	NT	NT	560	>10,000	>10,000
ZINC127859549	42,379	0.33	10,400	NT	NT	NT	NT	260	>10,000	3,570
ZINC437075156	1,542	0.34	10,400	NT	NT	NT	NT	190	>10,000	>10,000
ZINC130532671	89	0.3	IC$_{50}$ = 10,800	NT	NT	NT	NT	320	>10,000	>10,000
ZINC518842964	1,631	0.33	22,100	NT	NT	NT	NT	120	>10,000	>10,000
ZINC651262870	1,328	0.32	31,000	NT	NT	NT	NT	440	>10,000	>10,000
ZINC609076791	572	0.33	31,500	NT	NT	NT	NT	330	>10,000	>10,000
ZINC362128724	1,615	0.34	32,200	NT	NT	NT	NT	160	8,610	6,040
ZINC467716766	1,171	0.31	34,800	NT	NT	NT	NT	700	>10,000	>10,000
ZINC375299581	198	0.32	ND	NT	NT	NT	NT	180	>10,000	>10,000
ZINC247398558	225	0.35	ND	NT	NT	NT	NT	210	>10,000	>10,000
ZINC176752603	92	0.3	ND	NT	NT	NT	NT	300	>10,000	>10,000
ZINC480408888	75	0.34	ND	NT	NT	NT	NT	400	>10,000	>10,000
ZINC449156693	5,802	0.28	ND	NT	NT	NT	NT	760	>10,000	>10,000
ZINC640028109	255	0.29	ND	NT	NT	NT	NT	810	>10,000	>10,000
ZINC92642352	42,403	0.23	ND	NT	NT	NT	NT	820	>10,000	>10,000
ZINC572302473	577	0.29	ND	NT	NT	NT	NT	910	>10,000	>10,000
ZINC601953994	235	0.32	ND	NT	NT	NT	NT	980	>10,000	>10,000
ZINC615622500	204	0.34	ND	NT	3,074	NT	ND	150	>10,000	5,400
ZINC358506216	5,857	0.33	NT	NT	NT	NT	NT	250	5,880	6,540
ZINC415558697	17,674	0.27	NT	NT	NT	NT	NT	990	2,000	5,870
ZINC237938360	17,654	0.32	NT	NT	NT	NT	NT	180	5,720	1,070
Quinpirole	ND	ND	0.32	1.82	63.3	NT	1	14.2	ND	ND
Dopamine	ND	ND	0.65	0.91	79.4	NT	2 to G protein	6.30	ND	ND

The 36 highest-affinity hits are shown. See Supplementary Table 4 for all 549 compounds tested. See Supplementary Table 6 for novelty.

*Cluster rank, position in cluster head (see Methods) list sorted by DOCK score.

†Tc, Tanimoto coefficient to dopaminergic, serotonergic or adrenergic ligands from ChEMBL.

‡ND, not determined. The compound was tested but no measurable value was observed.

§NT, not tested.

nature research

Corresponding author(s): Brian K. Shoichet, Bryan L. Roth & John J. Irwin

Reporting Summary

Nature Research wishes to improve the reproducibility of the work that we publish. This form provides structure for consistency and transparency in reporting. For further information on Nature Research policies, see Authors & Referees and the Editorial Policy Checklist.

Statistical parameters

When statistical analyses are reported, confirm that the following items are present in the relevant location (e.g. figure legend, table legend, main text, or Methods section).

n/a	Confirmed	
☐	☒	The exact sample size (n) for each experimental group/condition, given as a discrete number and unit of measurement
☒	☐	An indication of whether measurements were taken from distinct samples or whether the same sample was measured repeatedly
☒	☐	The statistical test(s) used AND whether they are one- or two-sided *Only common tests should be described solely by name; describe more complex techniques in the Methods section.*
☒	☐	A description of all covariates tested
☒	☐	A description of any assumptions or corrections, such as tests of normality and adjustment for multiple comparisons
☐	☒	A full description of the statistics including central tendency (e.g. means) or other basic estimates (e.g. regression coefficient) AND variation (e.g. standard deviation) or associated estimates of uncertainty (e.g. confidence intervals)
☒	☐	For null hypothesis testing, the test statistic (e.g. F, t, r) with confidence intervals, effect sizes, degrees of freedom and P value noted *Give P values as exact values whenever suitable.*
☐	☒	For Bayesian analysis, information on the choice of priors and Markov chain Monte Carlo settings
☒	☐	For hierarchical and complex designs, identification of the appropriate level for tests and full reporting of outcomes
☒	☐	Estimates of effect sizes (e.g. Cohen's d, Pearson's r), indicating how they were calculated
☐	☒	Clearly defined error bars *State explicitly what error bars represent (e.g. SD, SE, CI)*

Our web collection on statistics for biologists may be useful.

Software and code

Policy information about availability of computer code

Data collection	DOCK3.7.2
Data analysis	XDS (Version June 1, 2017), AIMLESS 0.5.32 , MOLREP 11.5.02, COOT 0.8.8, REFMAC 5.8.0158, PHENIX 1.11.1, CCP4 7.0.045, GraphPad Prism 5.0, Qnifft 2.2, cheminfTools 1.0, RDKit 2015_Q3, R 3.4.0

For manuscripts utilizing custom algorithms or software that are central to the research but not yet described in published literature, software must be made available to editors/reviewers upon request. We strongly encourage code deposition in a community repository (e.g. GitHub). See the Nature Research guidelines for submitting code & software for further information.

Data

Policy information about availability of data

All manuscripts must include a data availability statement. This statement should provide the following information, where applicable:

- Accession codes, unique identifiers, or web links for publicly available datasets
- A list of figures that have associated raw data
- A description of any restrictions on data availability

Structures of AmpC β-lactamase determined with the new docking hits are available from the Protein Databank with accession numbers 6DPZ, 6DPY, 6DPX and 6DPT. The compounds docked in this study are freely available from our ZINC database, http://zinc15.docking.org. All active compounds are available either from

the authors or may be purchased from Enamine. Figures with associated raw data include: Fig. 2, electron density and reflection files are deposited with the PDB; Fig. 3, underlying activities are uploaded in a excel file; Fig. 4, underlying numbers are uploaded in a excel file; Extended Data Fig. 1, underlying numbers are supplied in Supplementary Table 1; Extended Data Fig. 5, underlying activities are uploaded in a excel file; Extended Data Fig. 6, raw clustering/no-clustering rank numbers are uploaded as Supplementary Table 8 and 9. Further underlying data are provided in Supplementary Tables 3 and 5 (aggregation assays for AmpC inhibitors and D4 ligands); Extended Data Table 1 (crystallographic data collection & refinement); Supplementary Tables 9-10 and Supplementary Data 12-14 (chemical purity of active ligands, and their spectra); Supplementary Data 11 and 14 (synthetic routes to compounds).

Field-specific reporting

Please select the best fit for your research. If you are not sure, read the appropriate sections before making your selection.

☒ Life sciences   ☐ Behavioural & social sciences   ☐ Ecological, evolutionary & environmental sciences

For a reference copy of the document with all sections, see nature.com/authors/policies/ReportingSummary-flat.pdf

Life sciences study design

All studies must disclose on these points even when the disclosure is negative.

Sample size	Figure 4a: sample size was determined by a Bayesian Prior modeling. (See Methods and Extended Data Figure 7)
Data exclusions	No data were excluded.
Replication	Figure 3d & 3e: The data are the mean ± SEM from three assays. Figure 4a: Cyan points represent the hit-rate means and standard errors at each docking energy bin, n = (47,121, 51, 38, 37, 40, 38, 36, 35, 36, 35, 35). Ext. Data Figure 1d: The data are the mean ± SD from 20 samples. Ext. Data Figure 4: The data are the mean ± SEM from three assays Ext. Data Figure 7e: Estimated hit-rate based on evaluation by the authors of the docked poses before any molecules were tested (brown: mean (n compound = 200, 220, 230, 230, 285, 235, 210, 230, 200) ± stddev. (n experts = 5,4,4,4,4,4,4,4,4)), the prior mean (green), and samples (n=200) from the prior (blue). Supplemental Data Table 3: The data are the mean ± SD from three assays Supplemental Data Table 6: The data are the mean ± SD from three assays Supplemental Data Table 8 & 9: The data are the mean ± SD from 4 strategies (see methods)
Randomization	Ext. Data Figure 1d: to investigate the effect of library size on the ability to enrich "ligands" among the top 1000 ranked compounds, 100000, 300000, 1000000, 3000000, 10000000, 30000000 and 100000000 sets of molecules were randomly selected from the full docking-ranked list and the number of ligands among the 1000 was counted. Each set was generated twenty times.
Blinding	Investigators were not blinded

Reporting for specific materials, systems and methods

Materials & experimental systems

n/a	Involved in the study
☒	Unique biological materials
☒	Antibodies
☐	☒ Eukaryotic cell lines
☒	Palaeontology
☒	Animals and other organisms
☒	Human research participants

Methods

n/a	Involved in the study
☒	ChIP-seq
☒	Flow cytometry
☒	MRI-based neuroimaging

Eukaryotic cell lines

Policy information about cell lines

Cell line source(s)	HEK293 T cells (ATCC CRL-11268)
Authentication	All cells used in this study are commercial and were obtained from vendors as indicated in the manuscript. HEK293T were certified mycoplasma free and authenticated by ATCC. Cells

were also validated by analysis of short tandem repeat (STR) DNA profiles and these profiles showed 100% match at the STR database from ATCC

Mycoplasma contamination

HEK293T (ATCC CRL-11268; 59587035) were certified mycoplasma free by ATCC.

Commonly misidentified lines
(See ICLAC register)

No commonly misidentified cell lines were used.